

Variational approach to the dynamics of dissipative quantum impurity models

Yi-Fan Qu,^{1,*} Martino Stefanini,^{2,†} Tao Shi,^{3,4} Tilman Esslinger,⁵
Sarang Gopalakrishnan,⁶ Jamir Marino,² and Eugene Demler¹

¹*Institute for Theoretical Physics, ETH Zurich, 8093 Zurich, Switzerland*

²*Institut für Physik, Johannes Gutenberg-Universität Mainz, D-55099 Mainz, Germany[‡]*

³*CAS Key Laboratory of Theoretical Physics, Institute of Theoretical Physics,
Chinese Academy of Sciences, Beijing 100190, China*

⁴*CAS Center for Excellence in Topological Quantum Computation & School of Physical Sciences,
University of Chinese Academy of Sciences, Beijing 100049, China*

⁵*Institute for Quantum Electronics & Quantum Center, ETH Zurich, 8093 Zurich, Switzerland*

⁶*Department of Electrical and Computer Engineering,
Princeton University Princeton, New Jersey 08540, USA*

(Dated: November 22, 2024)

Recent experiments with quantum simulators using ultracold atoms and superconducting qubits have demonstrated the potential of controlled dissipation as a versatile tool for realizing correlated many-body states. However, determining the dynamics of dissipative quantum many-body systems remains a significant analytical and numerical challenge. In this work, we focus on a dissipative impurity problem as a testbed for new methodological developments. We introduce an efficient non-perturbative framework that combines the superposition of Gaussian states (SGS) variational ansatz with the quantum trajectory approach to simulate open systems featuring a dissipative impurity. Applying this method to a spinful impurity subject to two-body losses and embedded in a bath of noninteracting fermions, we explore the full crossover from weak to strong dissipation regimes. The non-perturbative nature of the SGS ansatz allows us to thoroughly examine this crossover, providing comprehensive insights into the system’s behavior. In the strong dissipation regime, our approach reproduces the finding that localized two-body losses can induce the Kondo effect [arXiv:2406.03527], characterized by a slowdown of spin relaxation and an enhancement of charge conductance. Furthermore, we reveal an exotic “reverse conductance” phenomenon at zero potential bias – a counter-intuitive single-body effect resulting from intermediate dissipation and finite bandwidth. Finally, we investigate the formation of ferromagnetic domains and propose an extension to realize a higher-spin Kondo model using localized dissipation.

I. INTRODUCTION

Dissipative quantum physics has been an active area of research for several decades. Coupling a quantum system to an environment not only acts detrimentally by inducing decoherence and dephasing, but can also result in the onset of phase transitions, as in the celebrated case of the spin-boson model [1]. With the advent of ultracold quantum simulators, it has been realized that dissipation can be used as a tool for preparing correlated states of matter [2–10] (see also recent work on quantum simulators using superconducting qubits [11, 12]). These developments underscore that dissipation, while typically suppressing quantum coherence, can also give rise to novel phenomena without counterparts in unitary systems, such as non-equilibrium critical steady states [13, 14] and instances of quantum many-body Zeno physics [15–20].

Understanding dissipative systems poses significant analytical and numerical challenges. Various simulation methods have been employed, including perturbative techniques like the Keldysh formalism [21–25]

and non-perturbative approaches such as exact diagonalization (ED) [8, 26, 27], density matrix renormalization group (DMRG) [28–30], matrix product operators (MPOs) [31, 32], Bethe ansatz [33–36], and variational approaches [37, 38]. However, non-perturbative methods face significant challenges when applied to large non-integrable dissipative systems, since the dimension of the space of density matrices grows with the size of the system even faster than for pure states. Thus, an important goal of theoretical quantum physics has been the development of approximations that are still non-perturbative but are less computationally intensive.

A class of dissipative systems garnering increasing attention is that of dissipative impurities [25, 39–43], where dissipation is confined to a small region within a larger quantum system. As their unitary counterparts (such as the Kondo [44] and Anderson impurity models [45] and polarons [46, 47], to mention only a few), they represent an ideal playground to understand the effect of dissipation in a simplified setting. In this article, we present a non-perturbative framework that combines the superposition of Gaussian states (SGS) variational ansatz—which is efficient for impurity problems [48–50]—with the quantum trajectory approach [51–55]. This framework significantly accelerates numerical simulations of the dynamics in dissipative impurity systems and holds potential for application to other platforms featuring local dis-

* yifaqu@phys.ethz.ch

† mstefa@uni-mainz.de

‡ Y.-F. Q. and M. S. contributed equally to this work.

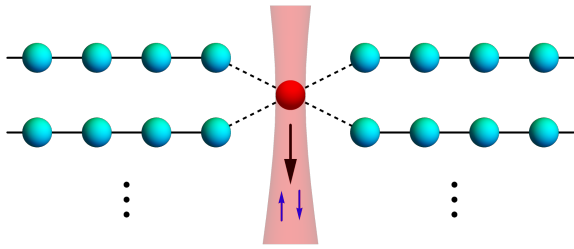


FIG. 1. Schematic of the setup with two-body dissipation at an impurity site, which is immersed in a spinful fermionic bath consisting of multiple channels.

sipation acting on an extended quantum system.

We apply our method to a dissipative impurity system where a spinful impurity, immersed in a bath of noninteracting fermions, undergoes two-body losses. Our approach effectively demonstrates that strong localized two-body losses give rise to the Kondo effect [56], in agreement with the analysis presented in the companion paper [57]. We characterize the emergence of Kondo physics by identifying two distinctive signatures: the slowdown of spin relaxation and the enhancement of charge conductance. Owing to the non-perturbative nature of the SGS ansatz, our method allows for a thorough examination of the full crossover from the weakly dissipative, mean-field regime to the strongly correlated Kondo regime, providing a comprehensive understanding of the system’s behavior across different dissipation regimes. Notably, in the mean-field regime, we reveal the emergence of exotic “reverse conductance” at zero potential bias, arising from intermediate dissipation and the constraints of a finite reservoir bandwidth. Furthermore, we explore a straightforward extension of the dissipative setup by introducing dissipation to multiple sites, enabling the realization of a spin-1 Kondo model. This development opens up new avenues for exploring higher-spin Kondo physics utilizing dissipation.

The paper is organized as follows. In Sec. II, we present the dissipative impurity model with two-body losses. Sec. III introduces the SGS framework for simulating open systems, which is combined with the quantum trajectory approach. In Sec. IV, we first benchmark our approach using ED. We then investigate the crossover to Kondo regimes through spin relaxation and conductance. In Sec. V, we demonstrate the origin of the “reverse conductance” phenomenon at zero potential bias. In Sec. VI we discuss the formation of ferromagnetic domains and the realization of high-spin Kondo models.

II. IMPURITY MODEL

We consider an impurity site immersed in a bath of noninteracting spinful fermions. As illustrated in Fig. 1, fermions on the central impurity site, can undergo a two-body loss: when two fermions with opposite spins occupy

this site, they can be lost from the system at a rate γ . Meanwhile, they can also tunnel into the bath, which consists of multiple channels (depicted by the cyan balls in Fig. 1). Assuming the losses are Markovian [58–61], the dynamics of the density matrix $\rho(t)$ of the system is described by a Lindblad master equation

$$\dot{\rho}(t) = -i[H, \rho(t)] + \gamma \left(L\rho(t)L^\dagger - \frac{1}{2}\{L^\dagger L, \rho(t)\} \right), \quad (1)$$

where the unitary part of the dynamics is governed by the Hamiltonian

$$\begin{aligned} H &= H_d + H_{\text{leads}} + H_{\text{tun}} \\ &= \varepsilon_d \sum_{\sigma} d_{\sigma}^{\dagger} d_{\sigma} + \sum_{p\sigma\alpha} \varepsilon_{p\alpha} c_{p\sigma\alpha}^{\dagger} c_{p\sigma\alpha} \\ &\quad + \sum_{p\sigma\alpha} (V_{p\alpha} d_{\sigma}^{\dagger} c_{p\sigma\alpha} + \text{H.c.}). \end{aligned} \quad (2)$$

Here, the d_{σ} operators represent the modes of spin σ with onsite energy ε_d at the impurity site. In the spinful fermionic bath, the $c_{p\sigma\alpha}$ operators correspond to the eigenmodes of channel α , which have single-particle energies $\varepsilon_{p\alpha} = \varepsilon_p - \mu_{\alpha}$ with momentum p and chemical potential μ_{α} . Fermions at the impurity site can tunnel into the bath via the hopping term H_{tun} with channel-dependent amplitudes $V_{p\alpha}$. The dissipative part of the dynamics in Eq. (1) is described by the jump operator $L = d_{\downarrow} d_{\uparrow}$, which represents two-body loss on the impurity site.

It is worth noting that our model is related to the well-known Anderson impurity model (AIM) described by the Hamiltonian

$$H_{\text{AIM}} = \varepsilon_d \sum_{\sigma} d_{\sigma}^{\dagger} d_{\sigma} + \frac{U_d}{2} d_{\uparrow}^{\dagger} d_{\uparrow} d_{\downarrow}^{\dagger} d_{\downarrow} + H_{\text{leads}} + H_{\text{tun}}, \quad (3)$$

where the impurity instead has onsite Coulomb repulsion with interaction strength U_d . In the AIM, a strong onsite repulsion generates correlations by imposing a constraint of no double occupancy on the impurity site. In our model (1), we achieve the same constraint by introducing a dissipation that actively removes double occupancies. However, we stress that in our model there are no interactions; all the correlations are introduced by two-body losses.

III. METHOD

In this section, we introduce and motivate the SGS variational ansatz in the context of closed systems. We then extend this method to open-system impurity models by using the quantum trajectory approach. The main achievement of our work is the combination of SGS with quantum trajectory, whose analytical details are presented in Sec. III C.

A. Superposition of Gaussian states ansatz

We begin by introducing the SGS ansatz for closed systems. Considering the AIM with Hamiltonian (3), the hybridization between the impurity and the bath leads to charge fluctuations at the impurity site. A general wave function can be expressed as a superposition of four states that feature different configurations in the impurity subspace, namely

$$|\Psi\rangle = \sum_{s=0,\uparrow,\downarrow,2} \alpha_s |s\rangle |\psi_s\rangle. \quad (4)$$

Here, $|s\rangle$ denotes the impurity states $|0\rangle$ (vacuum state), $|\uparrow\rangle$, $|\downarrow\rangle$, or $|2\rangle$ (double occupation), and $|\psi_s\rangle$ represents the corresponding many-body state of the bath. The coefficients α_s capture the entanglement between the impurity and the bath.

To gain intuition about the structure of the bath states $|\psi_s\rangle$, we first consider the case when the tunneling H_{tun} is turned off and the bath is in its ground state, the Fermi sea $|\text{FS}\rangle$. When the tunneling is turned on, the bath becomes connected to the impurity. As H_{tun} transfers electrons into and out of the bath, it generates both charge fluctuations and particle-hole excitations in the bath. This idea is the basis of the Gunnarson-Schönhammer ansatz, which was successfully employed to predict both the ground-state properties and the spectral function of the AIM [62]. A simple way to further improve the ansatz is to assume Gaussian states for the baths within different impurity subsectors, namely an ansatz using a superposition of four Gaussian states:

$$|\Psi_{\text{SGS}}\rangle = \sum_{s=0,\uparrow,\downarrow,2} \alpha_s |s\rangle |\text{GS}_s\rangle, \quad (5)$$

which increases the number of variational parameters while remaining numerically efficiently. Here, the Gaussian state $|\text{GS}_s\rangle$ corresponds to a single Slater determinant and can capture the particle-hole excitations non-perturbatively, which will be precisely defined in Sec. III C. To describe closed-system dynamics, we consider α and $|\text{GS}_s\rangle$ to be time-dependent. The technical details of implementing the real-time variational SGS ansatz are also discussed in Sec. III C.

It should be noted that Bravyi and Gosset [48] have shown that the ground state of an impurity Hamiltonian, up to a small fixed error, can be approximated as a superposition of a few Gaussian states, with the number of states scaling polynomially with the size of the bath. The SGS ansatz (5) used in our work can be considered as a “minimal version” of the most general SGS and thus highly efficient. The variational SGS has been implemented in closed systems and has been shown to capture both ground-state [49] and dynamical properties [50].

The SGS ansatz works well with pure states, both in and out of equilibrium. For our dissipative problem—and

more generally—we aim to further extend it to open-system impurity problems. The simplest way is to employ the quantum trajectory approach, which allows approximating a mixed state with an ensemble of pure states. This enables the direct use Eq. (5). To explore the dynamics governed by the master equation (1), we focus exclusively on real-time evolution, starting from a pure state of the entire system.

B. Quantum trajectory approach

In this subsection, to make our work self-contained, we briefly revisit the quantum trajectory approach, previously detailed in the literature [51–55].

Considering the master equation (1), we rewrite it as

$$\frac{d}{dt}\rho = -i(H_{\text{NH}}\rho - \rho H_{\text{NH}}^\dagger) + \gamma L^\dagger \rho L, \quad (6)$$

with a non-Hermitian Hamiltonian

$$H_{\text{NH}} = H - i\frac{\gamma}{2}L^\dagger L. \quad (7)$$

It has been proven that Eq. (6) can be reproduced by the following unraveling procedure. For simplicity, we assume that the initial density operator $\rho(t=0) = |\psi_0\rangle\langle\psi_0|$ is a pure state, with $|\psi_0\rangle$ denoting the normalized initial wave function. Then, one forms an ensemble of N_{Traj} quantum trajectories $|\psi_i(t)\rangle$ by evolving $|\psi_0\rangle$ with H_{NH} , and interspersing the evolution with discontinuous quantum jumps $|\psi_i(t^+)\rangle = L|\psi_i(t^-)\rangle / \|L|\psi_i(t^-)\rangle\|$ according to certain probabilistic rules. The average state of the ensemble thus constructed,

$$\rho(t) = \frac{1}{N_{\text{Traj}}} \sum_{i=1}^{N_{\text{Traj}}} \frac{|\psi_i(t)\rangle\langle\psi_i(t)|}{\langle\psi_i(t)|\psi_i(t)\rangle}, \quad (8)$$

converges to the solution of Eq. (6) as $N_{\text{Traj}} \rightarrow \infty$. In a concrete simulation with a finite N_{Traj} , Eq. (8) provides an approximation to the desired $\rho(t)$.

Following Ref. [63], we outline the main procedures on how to obtain $|\psi_i(t)\rangle$: (a) Draw a uniformly distributed random number r from $[0, 1]$. (b) Solve the non-Hermitian real-time evolution $|\psi_i(t)\rangle = \exp(-iH_{\text{NH}}t)|\psi_0\rangle$ with the initial state $|\psi_0\rangle$ and the non-Hermitian Hamiltonian. (c) Solve equation $\| |\psi_i(t)\rangle \|^2 = r$ numerically to find the time t_1 when the quantum jump occurs. (d) At time t_1 , apply the jump and then normalize the new wave function as $|\psi_i(t_1^+)\rangle = L|\psi_i(t_1^-)\rangle / \|L|\psi_i(t_1^-)\rangle\|$. (e) Continue the time evolution from step (a) by sampling a new random number r and replacing the initial state with $|\psi_i(t_1^+)\rangle$.

The expectation value of an observable \hat{O} is obtained by taking the average over the contributions from all trajectories, namely

$$O(t) \equiv \text{Tr}(\hat{O}\rho(t)) = \frac{1}{N_{\text{Traj}}} \sum_{i=1}^{N_{\text{Traj}}} O_i(t), \quad (9)$$

with $O_i(t) \equiv \langle \psi_i(t) | \hat{O} | \psi_i(t) \rangle / \langle \psi_i(t) | \psi_i(t) \rangle$ being the expectation value for a single trajectory i . For large but finite N_{Traj} , the statistical error of $O(t)$

$$\sigma_O = \frac{\Delta O}{\sqrt{N_{\text{Traj}}}} \quad (10)$$

asymptotically approaches zero, as $\sigma_O \sim N_{\text{Traj}}^{-1/2}$. Here, $\Delta O = \sum_i (O_i - O)^2 / N_{\text{Traj}}$ is the standard deviation, which generally converges as $N_{\text{Traj}} \rightarrow \infty$.

The quantum trajectory approach has the advantage of evolving pure states of dimension $N_{\mathcal{H}}$ instead of the density operator of dimension $N_{\mathcal{H}}^2$, where the Hilbert space dimension $N_{\mathcal{H}}$ generally increases exponentially with the size of the system. Therefore, it is very efficient for solving open-system quantum problems. The trade-off is the introduction of statistical errors resulting from the (classical) fluctuations in the sampling of a finite number of trajectories. Nevertheless, there is no sign problem in this approach (each trajectory carries equal and positive weight), so the errors can be well controlled by increasing the number of trajectories.

C. Variational techniques

In this subsection, we provide the technical details of implementing our open-quantum-system SGS approach. The SGS ansatz (5) consists of a superposition of four direct product states $|s\rangle |\text{GS}_s\rangle$ in different impurity sectors. Between two successive quantum jumps, the non-Hermitian Hamiltonian (7) for describing the dynamics explicitly reads $H_{\text{NH}} = H - i\frac{\gamma}{2}n_{d\uparrow}n_{d\downarrow}$, which is exactly the AIM (see Eq. (3)) with an imaginary interaction. The total fermion number $N_{\text{tot}} = \sum_{j\sigma\alpha} c_{j\sigma\alpha}^\dagger c_{j\sigma\alpha}$ is conserved, since it commutes with H_{NH} . The Gaussian state in the SGS ansatz is defined by

$$|\text{GS}_s(t)\rangle \equiv e^{iC^\dagger \xi_s(t)C} |\text{Fock}_s\rangle, \quad (11)$$

which has a definite particle number $N_s = N_{\text{tot}}, N_{\text{tot}} - 1, N_{\text{tot}} - 2$ for $s = 0, \uparrow (\downarrow), 2$, respectively. Denoting by N_f the number of bath modes, the variational parameter ξ_s is a $N_f \times N_f$ Hermitian matrix which means the SGS ansatz (5) has $O(N_f^2)$ variational parameters. The column vector $C = (c_1, c_2, \dots, c_{N_f})^T$ is a shorthand for the ordered combination of all annihilation operators $c_{p\sigma\alpha}$ in the bath. Without loss of generality, the Fock state $|\text{Fock}_s\rangle$ is fixed to $C_1^\dagger C_2^\dagger \dots C_{N_s}^\dagger |0_{\text{bath}}\rangle$, in which the first N_s modes on top of the vacuum state $|0_{\text{bath}}\rangle$ of the leads are occupied. For clarity, we note that the Gaussian state (11) with a definite particle number can be put in the standard Slater determinant form as $|\text{GS}_s\rangle = \bar{C}_1^\dagger \bar{C}_2^\dagger \dots \bar{C}_{N_s}^\dagger |0\rangle$ by letting $e^{iC^\dagger \xi_s C}$ transform the bath modes C to $\bar{C}^\dagger = C^\dagger U_s$ with $U_s = \exp(i\xi_s)$.

To employ the quantum trajectory approach, we need two ingredients: how to solve the non-Hermitian

evolution between quantum jumps and how to implement these quantum jumps. Let us start with the non-Hermitian evolution. The variational dynamics can be determined by minimizing the variational error $\left\| \frac{d}{dt} |\Psi_{\text{SGS}}\rangle + iH_{\text{NH}} |\Psi_{\text{SGS}}\rangle \right\|$ at each time, which gives the (non-Hermitian) projective Schrödinger equation

$$\frac{d}{dt} |\Psi_{\text{SGS}}\rangle = -iP_{\mathcal{T}} H_{\text{NH}} |\Psi_{\text{SGS}}\rangle. \quad (12)$$

Here, $P_{\mathcal{T}}$ projects any state into the tangent space of the variational manifold, which has orthonormal basis vectors $|s\rangle |\text{GS}_s\rangle$ and $e^{iC^\dagger \xi_s C} C_{j'}^\dagger C_j |s\rangle |\text{Fock}_s\rangle$ with $j \in \mathcal{I}_{\mathcal{P}}, j' \in \mathcal{I}_{\mathcal{H}}$. The indices $\mathcal{I}_{\mathcal{P}} = \{N_s + 1, \dots, N_f\}$ correspond to the created particles (indexed by j) on top of $|\text{Fock}_s\rangle$. Analogously, the indices $\mathcal{I}_{\mathcal{H}} = \{1, \dots, N_s\}$ correspond to the generated holes (indexed by j').

Choosing α_s and $U_s = \exp(i\xi_s)$ as time-dependent variational parameters, the left-hand side of Eq. (12) can be expressed as [64]

$$\frac{d}{dt} |\Psi_{\text{SGS}}\rangle = \sum_s e^{iC^\dagger \xi_s C} \left[\dot{\alpha}_s + \alpha_s C^\dagger U_s^\dagger \dot{U}_s C \right] |s\rangle |\text{Fock}_s\rangle. \quad (13)$$

In the formula above, we notice that $c_{j_1}^\dagger c_{j_2} |\text{Fock}_s\rangle = 0$ for $j_2 \in \mathcal{I}_{\mathcal{P}}$ gives a trivial contribution and $c_{j_1}^\dagger c_{j_2} |\text{Fock}_s\rangle = \delta_{j_1 j_2} |\text{Fock}_s\rangle$ for $j_1, j_2 \in \mathcal{I}_{\mathcal{H}}$ gives the same contribution as the $\dot{\alpha}_s$ term. This means that there are redundancies in the variational parameters, namely multiple sets of $\dot{\alpha}_s$ and \dot{U}_s that give the same physical state on the right-hand side of Eq. (12). To remove these redundancies, it is sufficient to apply the constraints

$$\begin{aligned} (U_s^\dagger \dot{U}_s)_{\mathcal{I}_{\mathcal{H}} \mathcal{I}_{\mathcal{H}}} &= 0_{N_s \times N_s}, \\ (U_s^\dagger \dot{U}_s)_{\mathcal{I}_{\mathcal{P}} \mathcal{I}_{\mathcal{P}}} &= 0_{(N_f - N_s) \times (N_f - N_s)}. \end{aligned} \quad (14)$$

These constraints are applied to the hole and particle subblocks in matrix $U_s^\dagger \dot{U}_s$.

The equations of motion (EoMs) for $\dot{\alpha}_s$ and \dot{U}_s are determined by taking the overlap between $-iH_{\text{NH}} |\Psi_{\text{SGS}}\rangle$ and the tangential basis:

$$\begin{aligned} \dot{\alpha}_s &= -i \langle \text{GS}_s | \langle s | H_{\text{NH}} | \Psi_{\text{SGS}} \rangle, \\ (U_s^\dagger \dot{U}_s)_{jj'} &= -i \alpha_s^{-1} \langle \text{GS}_s | \langle s | c_{j'}^\dagger c_j H_{\text{NH}} | \Psi_{\text{SGS}} \rangle \end{aligned} \quad (15)$$

with $j \in \mathcal{I}_{\mathcal{P}}$ and $j' \in \mathcal{I}_{\mathcal{H}}$. The other elements are fully fixed by the constraints in Eq. (14) and the unitarity of U_s , which gives $(U_s^\dagger \dot{U}_s)^\dagger = -U_s^\dagger \dot{U}_s$. To evaluate the right-hand side of Eq. (15), we need to calculate the action of H_{NH} , which can be recast as $H_{\text{NH}} = \bar{H}_{\text{imp}} + H_{\text{leads}} + H_{\text{tun}}$ with $\bar{H}_{\text{imp}} = H_{\text{imp}} - i\frac{\gamma}{2}n_{d\uparrow}n_{d\downarrow}$. The action of \bar{H}_{imp} is straightforward as it acts only on the impurity site. The contribution of H_{leads} can easily be obtained utilizing the Wick contraction theorem for the individual Gaussian state $|\text{GS}_s\rangle$. The action of H_{tun} is the only action that results in a variational error and is nontrivial because it has matrix elements between different impurity states. Meanwhile, it generates new Gaussian states through a

single annihilation (creation) operator \bar{c}_σ (\bar{c}_σ^\dagger) with $\bar{c}_\sigma = \sum_{p\alpha} V_{p\alpha} c_{p\sigma\alpha}$, namely

$$\begin{aligned}\bar{c}_\sigma |\text{GS}_s\rangle &= \beta_{\sigma s}^- |\text{GS}_{\sigma s-}\rangle, \\ \bar{c}_\sigma^\dagger |\text{GS}_s\rangle &= \beta_{\sigma s}^+ |\text{GS}_{\sigma s+}\rangle.\end{aligned}\quad (16)$$

Here, the generated state $|\text{GS}_{\sigma s\mp}\rangle$ and the relevant coefficient $\beta_{\sigma s}^\mp$ are obtained by manipulating the occupied modes of $|\text{GS}_s\rangle$ (see Appendix A for details). Finally, we need to calculate the overlaps between the different Gaussian states, which can be derived through the following expressions [65, 66]:

$$\mathcal{O}_{\lambda,\lambda'} = \langle \text{GS}_\lambda | \text{GS}_{\lambda'} \rangle = \det(u_\lambda^\dagger u_{\lambda'}), \quad (17a)$$

$$\begin{aligned}(\varrho_{\lambda,\lambda'})_{ij} &= \langle \text{GS}_\lambda | C_i^\dagger C_j | \text{GS}_{\lambda'} \rangle \\ &= \mathcal{O}_{\lambda,\lambda'} \left[u_{\lambda'} \left(u_\lambda^\dagger u_{\lambda'} \right)^{-1} u_\lambda^\dagger \right]_{ji} \\ &= \left[u_{\lambda'} \text{adj}(u_\lambda^\dagger u_{\lambda'}) u_\lambda^\dagger \right]_{ji},\end{aligned}\quad (17b)$$

where $|\text{GS}_\lambda\rangle$ and $|\text{GS}_{\lambda'}\rangle$, having the same particle number \mathcal{N}_λ , denote the two different Gaussian states. The $N_f \times \mathcal{N}_\lambda$ matrix u_λ ($u_{\lambda'}$), representing the first \mathcal{N}_λ columns of U_λ ($U_{\lambda'}$), consists of all orthonormal modes occupied in the state $|\text{GS}_\lambda\rangle$ ($|\text{GS}_{\lambda'}\rangle$). The last line of Eq. (17b) can be applied even if the matrix $u_\lambda^\dagger u_{\lambda'}$ is not invertible, where $\text{adj}(\dots)$ represents the adjugate of a square matrix.

Following the steps outlined above and using equations (16) and (17), we finally obtain the EoMs (15) for the variational parameters between two quantum jumps:

$$\dot{\alpha}_s = -i \left(n_s \epsilon_d + E_s - i \frac{\gamma}{2} \delta_{s2} \right) \alpha_s + f_s, \quad (18a)$$

$$\dot{U}_s = -i U_s \mathcal{A}_s, \quad (18b)$$

where $n_s \equiv \langle s | n_{d\uparrow} + n_{d\downarrow} | s \rangle$ is the particle number of the impurity and

$$E_s = \langle \text{GS}_s | H_{\text{leads}} | \text{GS}_s \rangle = \text{Tr} \left(U_s^\dagger h U_s \right)_{\mathcal{H}\mathcal{H}}, \quad (19a)$$

$$\mathcal{A}_s = \begin{bmatrix} 0_{N_s \times N_s} & [U_s^\dagger (h + \mathcal{F}_s) U_s]_{\mathcal{H}\mathcal{P}} \\ [U_s^\dagger (h + \mathcal{F}_s) U_s]_{\mathcal{P}\mathcal{H}} & 0_{(N_f - N_s) \times (N_f - N_s)} \end{bmatrix}. \quad (19b)$$

Here, the Hermitian matrix h is defined by rewriting $H_{\text{leads}} = C^\dagger h C$. The variables f_s and F_s originate from the tunneling events, and are summarized below:

$$\begin{aligned}f_0 &= \alpha_\uparrow \beta_{\uparrow\uparrow}^+ \mathcal{O}_{0,\uparrow\uparrow+} + \alpha_\downarrow \beta_{\downarrow\downarrow}^+ \mathcal{O}_{0,\downarrow\downarrow+}, \\ f_\uparrow &= \alpha_0 \beta_{\uparrow 0}^- \mathcal{O}_{\uparrow,\uparrow 0-} + \alpha_2 \beta_{\downarrow 2}^+ \mathcal{O}_{\uparrow,\downarrow 2+}, \\ f_\downarrow &= \alpha_0 \beta_{\downarrow 0}^- \mathcal{O}_{\downarrow,\downarrow 0-} - \alpha_2 \beta_{\uparrow 2}^+ \mathcal{O}_{\downarrow,\uparrow 2+}, \\ f_2 &= \alpha_\uparrow \beta_{\downarrow\uparrow}^- \mathcal{O}_{2,\downarrow\uparrow-} - \alpha_\downarrow \beta_{\uparrow\downarrow}^- \mathcal{O}_{2,\uparrow\downarrow-},\end{aligned}\quad (20)$$

and

$$\begin{aligned}\mathcal{F}_0 &= \alpha_0^{-1} \left(\alpha_\uparrow \beta_{\uparrow\uparrow}^+ \varrho_{0,\uparrow\uparrow+} + \alpha_\downarrow \beta_{\downarrow\downarrow}^+ \varrho_{0,\downarrow\downarrow+} \right), \\ \mathcal{F}_\uparrow &= \alpha_\uparrow^{-1} \left(\alpha_0 \beta_{\uparrow 0}^- \varrho_{\uparrow,\uparrow 0-} + \alpha_2 \beta_{\downarrow 2}^+ \varrho_{\uparrow,\downarrow 2+} \right), \\ \mathcal{F}_\downarrow &= \alpha_\downarrow^{-1} \left(\alpha_0 \beta_{\downarrow 0}^- \varrho_{\downarrow,\downarrow 0-} - \alpha_2 \beta_{\uparrow 2}^+ \varrho_{\downarrow,\uparrow 2+} \right), \\ \mathcal{F}_2 &= \alpha_2^{-1} \left(\alpha_\uparrow \beta_{\downarrow\uparrow}^- \varrho_{2,\downarrow\uparrow-} - \alpha_\downarrow \beta_{\uparrow\downarrow}^- \varrho_{2,\uparrow\downarrow-} \right),\end{aligned}\quad (21)$$

where we have introduced the notation $\mathcal{O}_{s,\lambda}$ and $\varrho_{s,\lambda}$, with s and λ denoting the index of $|\text{GS}_s\rangle$ and $|\text{GS}_{\sigma s'\pm}\rangle$, respectively.

The only missing ingredient is how to implement quantum jumps that occur randomly during evolution. Due to the local nature of the jump operator L , the effect of quantum jumps on the SGS is simple: every impurity state will be annihilated, except for $|2\rangle$, which is then mapped to $|0\rangle$. Correspondingly, assuming the quantum jump occurs at t_1 , the variational parameters should be updated by

$$\begin{aligned}\alpha_0(t_1^+) &= \alpha_2(t_1^-), \quad \alpha_{\uparrow,\downarrow,2}(t_1^+) = 0, \\ U_0(t_1^+) &= U_2(t_1^-).\end{aligned}\quad (22)$$

To determine $U_{\uparrow,\downarrow,2}(t_1^+)$, we consider the evolution over a short time interval after the jump, utilizing the Taylor expansion of the non-Hermitian evolution (see Appendix B).

In summary, the SGS techniques, with $O(N_f^2)$ variational parameters, can efficiently implement non-Hermitian evolution and quantum jumps in the quantum trajectory approach. This variational method, as shown in the following sections, is non-perturbative and works well in different regimes of loss rate γ . Our method can also be directly generalized to other impurity problems in an open system, with a superconducting bath; a superfluid bosonic bath; or multiple impurity sites (or quantum dots), etc.

IV. RESULTS: CROSSOVER TO KONDO REGIME

In this section, we apply our SGS approach to a specific implementation of the model outlined in Sec. II: we consider two reservoirs modeled as two chains of nearest-neighbor hopping fermions with open boundary conditions, connected to the dot site at one end:

$$\begin{aligned}H_{\text{leads}} &= -J \sum_{\alpha=L,R} \sum_{j=1}^{\ell-1} \sum_{\sigma} (c_{j+1\sigma\alpha}^\dagger c_{j\sigma\alpha} + \text{H.c.}) \\ &\quad - \sum_{\alpha=L,R} \sum_{j=1}^{\ell} \sum_{\sigma} \mu_\alpha c_{j\sigma\alpha}^\dagger c_{j\sigma\alpha}\end{aligned}\quad (23a)$$

$$H_{\text{tun}} = -V \sum_{\alpha=L,R} \sum_{\sigma} (d_\sigma^\dagger c_{1\sigma\alpha} + \text{H.c.}), \quad (23b)$$

where ℓ is the size of each chain, J is the hopping amplitude of the fermions in the bath, and V is the tunneling amplitude. The channel index $\alpha = L, R$ represents the left and right reservoirs. This choice of the leads is not particularly restrictive, since impurity problems can always be reduced to a collection of one-dimensional (1D) channels [67, 68]. The leads' Hamiltonian can be diagonalized by $c_{j\sigma\alpha} = \sum_p \psi_p(j) c_{p\sigma\alpha}$, with $\psi_p(j) = \sqrt{\frac{2}{\ell+1}} \sin pj$ where $p \in \{\frac{\pi}{\ell+1}n | n = 1 \dots \ell\}$. The resulting dispersion and impurity-lead tunneling are

$$\varepsilon_{p\alpha} = -2J \cos p - \mu_\alpha, \quad (24a)$$

$$V_{p\alpha} = -V \psi_p(1) = -\sqrt{\frac{2}{\ell+1}} V \sin p. \quad (24b)$$

Through Fermi's golden rule, the tunneling rate associated with the α channel is given by

$$\begin{aligned} \Gamma_\alpha(\omega) &= 2\pi \sum_p |V_{p\alpha}|^2 \delta(\omega - \varepsilon_{p\alpha}) \\ &= \frac{2V^2}{J} \sqrt{1 - \frac{(\omega - \mu_\alpha)^2}{4J^2}} \end{aligned} \quad (25)$$

for $|\omega - \mu_\alpha| \leq 2J$ and zero otherwise. The total tunneling rate of the impurity is then given by $\Gamma(\omega) = \Gamma_L(\omega) + \Gamma_R(\omega)$.

We employ the SGS approach to show how the Kondo effect emerges as a consequence of the localized two-body losses by characterizing two signatures of Kondo physics: spin relaxation and charge conductance. In both cases, the non-perturbative nature of the SGS ansatz allows us to examine the full crossover from small to large γ .

A. Benchmark of the variational approach

We begin by applying the SGS approach to a small system (with the size of each chain being $\ell = 5$) and comparing the results under varying dissipation rates γ with the exact results obtained using exact diagonalization (ED). We fix the chemical potentials and the on-site potential of the impurity to $\mu_L = \mu_R = \varepsilon_d = 0$, so that the system is at half filling. The tunneling amplitude is set to $V = J$. It should be noted that the system exhibits parity symmetry, characterized by the interchangeability of the channels L and R . Therefore, the impurity will only couple to the symmetric bath modes $c_{i\sigma e} = (c_{i\sigma L} + c_{i\sigma R})/\sqrt{2}$, while the asymmetric bath modes $c_{i\sigma o} = (c_{i\sigma L} - c_{i\sigma R})/\sqrt{2}$ are decoupled. The two-channel model (23) is then mapped to a one-channel model with the tunneling amplitude replaced by $\sqrt{2}V$. In both ED (performed with the QuTiP package [69, 70]) and SGS calculations, we only consider 6 symmetric sites, including the impurity site.

To simulate the dynamics, we first turn off the dissipation and prepare the whole system in the ground state,

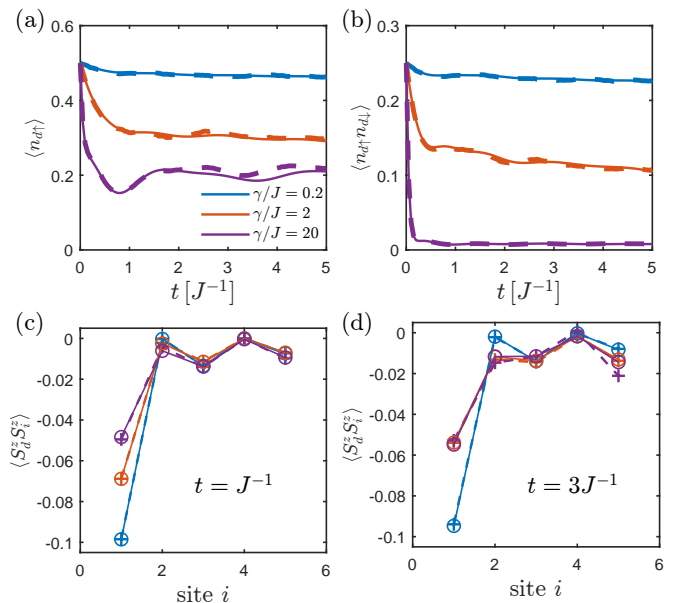


FIG. 2. Benchmark between the SGS approach (dashed curve) and the ED approach (solid curve) in a small system of $\ell = 5$. We consider only the symmetric modes. The dissipation is first turned off and the system is prepared in the ground state with the numbers of spin-up and spin-down particles being $N_{\text{tot},\uparrow} = N_{\text{tot},\downarrow} = 3$. Then the dissipation is quenched to a finite value, and the state starts evolving. (a) and (b) show the time-dependent $\langle n_{d\uparrow} \rangle$ and $\langle n_{d\uparrow} n_{d\downarrow} \rangle$, in which the quantum Zeno effect occurs for $\langle n_{d\uparrow} n_{d\downarrow} \rangle$ at $\gamma/J = 20$. (c) and (d) show spin- z correlation between the impurity and bath sites at different times $t = J^{-1}$ and $t = 3J^{-1}$, which exhibit antiferromagnetic signatures. The parameters used are $V = J, \mu_L = \mu_R = \varepsilon_d = 0$, and $N_{\text{Traj}} = 1000$.

with the total numbers of the spin-up and spin-down particles being $N_{\text{tot},\uparrow} = N_{\text{tot},\downarrow} = 3$. We then quench the dissipation to a finite value and let the state evolve under the master equation (1). In Figs. 2(a) and 2(b), we show the time-dependent expectation values of the spin-up particle occupation $\langle n_{d\uparrow} \rangle$ and the double occupancy $\langle n_{d\uparrow} n_{d\downarrow} \rangle$, which can be directly obtained from our SGS ansatz (5). These physical quantities capture how two-body dissipation affects particle occupations on the impurity site. For a low dissipation rate $\gamma = 0.2J$ (blue curves), $\langle n_{d\uparrow} \rangle$ and $\langle n_{d\uparrow} n_{d\downarrow} \rangle$ are almost unchanged during the evolution, as the system is close to the non-dissipative case of $\gamma = 0$, whose ground state can be exactly expressed by the SGS ansatz. For an intermediate dissipation rate $\gamma = 2J$ (orange curves), both $\langle n_{d\uparrow} n_{d\downarrow} \rangle$ and $\langle n_{d\uparrow} \rangle$ display a two-step dynamics, with a steeper transient followed by a slower decay. We find the transient in the double occupancies occurs with a rate $\sim \gamma$, while the spin-up occupation decays more slowly with a rate $\sim \gamma/2$. This difference in timescales between $\langle n_{d\uparrow} \rangle$ and $\langle n_{d\uparrow} n_{d\downarrow} \rangle$ can be understood by considering that weak two-body losses do not impart strong correlations between spin-up and spin-down sectors, so we can estimate $\langle n_{d\uparrow} n_{d\downarrow} \rangle \simeq \langle n_{d\uparrow} \rangle \langle n_{d\downarrow} \rangle = \langle n_{d\uparrow} \rangle^2$. Therefore, the decay rate of $\langle n_{d\uparrow} n_{d\downarrow} \rangle$ is about twice that

of $\langle n_{d\uparrow} \rangle$, namely $\frac{d}{dt} \langle n_{d\uparrow} n_{d\downarrow} \rangle / \langle n_{d\uparrow} n_{d\downarrow} \rangle \simeq 2 \frac{d}{dt} \langle n_{d\uparrow} \rangle / \langle n_{d\uparrow} \rangle$. For a high dissipation rate $\gamma = 20J$ (purple curves), $\langle n_{d\uparrow} n_{d\downarrow} \rangle$ drops dramatically at first and then remains nearly zero, which is a clear signature of the quantum Zeno effect due to the fast decay of the double occupation state $|\uparrow\downarrow\rangle$ on the impurity site. However, the dynamics of $\langle n_{d\uparrow} \rangle$ has two stages corresponding to different energy scales: the first stage is the fast decay with a rate of γ within the initial short time interval $t \lesssim \gamma^{-1}$, resulting from the rapid two-body decay of the impurity state $|\uparrow\downarrow\rangle$. The second stage is a slower decrease followed by slight fluctuations around an average value, which results from charge tunneling and fluctuations within the impurity sectors $|0\rangle$ and $|\uparrow\rangle$. For all regimes of γ , the SGS results agree well with the ED results, although $\langle n_{d\uparrow} \rangle$ shows slightly larger discrepancies for $\gamma = 20J$ after a long time evolution when $t \gtrsim 2.5J^{-1}$.

To further testify the accuracy of our approach, we investigated the spin- z correlation functions between the impurity site and the bath sites at two distinct times, $t = J^{-1}$ and $t = 3J^{-1}$. These correlations are denoted as $\langle S_d^z S_i^z \rangle$, in which $S_d^a = \frac{1}{2} \sum_{\sigma\sigma'} d_{\sigma}^{\dagger} \tau_{\sigma\sigma'}^a d_{\sigma'}$ and $S_i^a = \frac{1}{2} \sum_{\sigma\sigma'} c_{i\sigma e}^{\dagger} \tau_{\sigma\sigma'}^a c_{i\sigma' e}$ (with the Pauli matrices τ^a) represent the spin operators of the impurity and the symmetric bath site i , respectively. As presented in Figs. 2(c) and 2(d), $\langle S_d^z S_i^z \rangle$ is negative, indicating antiferromagnetic (AF) signatures for different dissipation rates, especially for odd bath sites. At $t = J^{-1}$, the magnitude of $\langle S_d^z S_1^z \rangle$ decreases with increasing γ , showing that the two-body loss on the impurity site tends to suppress the AF correlations present in the ground state with $\gamma = 0$. This phenomenon can be explained as follows [8]. For simplicity, consider only the impurity site and the first bath site, initialized in an AF state $|\uparrow\rangle_{\text{imp}} |\downarrow\rangle_1$. This state can be transferred to the double occupation state $|\uparrow\downarrow\rangle_{\text{imp}} |0\rangle_1$ through tunneling H_{tun} , thus it will undergo dissipation to $|0\rangle_{\text{imp}} |0\rangle_1$, which is nonmagnetic. Indeed, it is known that two-body losses remove pairs of fermions in a singlet state [8, 71]—since only the singlet component of $|\uparrow\rangle_{\text{imp}} |\downarrow\rangle_1$ is connected to $|\uparrow\downarrow\rangle_{\text{imp}} |0\rangle_1$ —thereby tending to suppress AF ordering. Therefore, AF correlations are weaker with a higher dissipation rate γ .

In summary, our approach captures different occupation numbers and spin correlations describing the impurity cloud. Quantitatively, there is good agreement between our results and the ED results, clearly demonstrating the accuracy of our SGS ansatz. Furthermore, the approach is capable of showing the full crossover from small to large γ .

B. Spin relaxation: crossover from the mean-field regime to the Kondo regime

We now focus on the first Kondo signature: impurity's spin relaxation slows down with increasing γ [57]; in the Kondo regime, the lifetime of the impurity's magnetization is $1/T_K$, where T_K is the Kondo temperature.

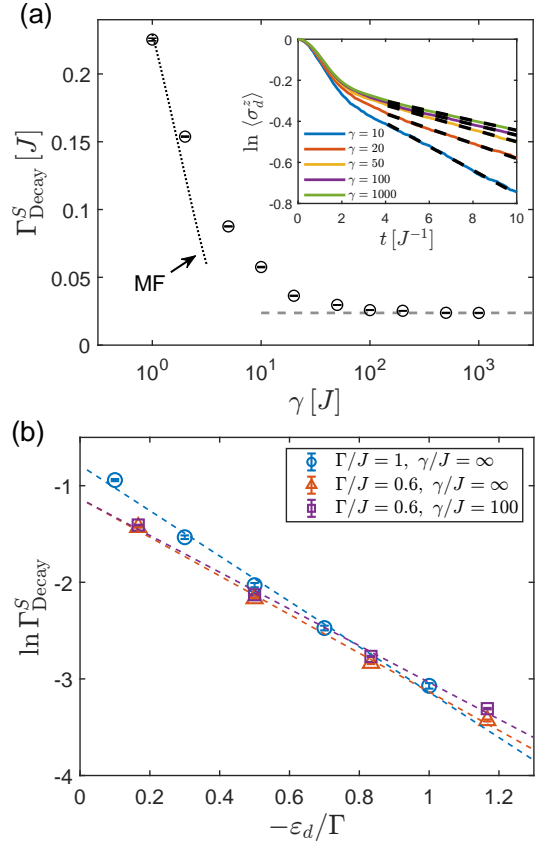


FIG. 3. Spin relaxation. (a): the decay rate Γ_{Decay}^S (extracted from dynamics in the inset) versus dissipation rate γ . In the large γ regime, the relaxation rate Γ_{Decay}^S converges, displaying a plateau as depicted by the dashed curve. This plateau indicates the Kondo regime with two-body losses. In the small γ regime, the SGS results closely align with the mean-field results (dotted line). The inset shows the real time dynamics of the impurity magnetization $\langle \sigma_d^z \rangle = \langle n_{d\uparrow} \rangle - \langle n_{d\downarrow} \rangle$, which exhibits decay behavior $\langle \sigma_d^z \rangle \sim e^{-\Gamma_{\text{Decay}}^S t}$ at large times. The system size for the SGS simulations is set to $\ell = 60$, with $\varepsilon_d = -0.5J$. (b): spin decay rate versus ε_d . The collapse of different curves shows the universal behavior (at large dissipation) $\Gamma_{\text{Decay}}^S \sim \exp(-\eta\pi|\varepsilon_d|/\Gamma)$ with a coefficient $\eta \sim 0.61$, while the RG prediction at $\gamma = \infty$ is $\eta_{\text{RG}} = 1$ [72]. The discrepancy results from the renormalization of the effective spin interaction between the impurity site fermion and itinerant fermions by higher-order processes in Γ/ε_d .

To capture spin relaxation with the SGS approach, we consider a larger system ($\ell = 60$) with an onsite potential $\varepsilon_d < 0$. The chemical potentials are fixed to $\mu_L = \mu_R = 0$, so the system is around half filling and only the symmetric modes need to be considered. To simulate the dynamics, we first turn off both dissipation and tunneling H_{tun} , i.e., set $\gamma = V = 0$. The system is prepared as a disentangled static state $|\uparrow\rangle |\text{FS}\rangle$, combining a spin-up impurity and the Fermi sea of the bath. Then we suddenly turn on both γ and V , and the magnetization of the impurity, denoted by $\langle \sigma_d^z \rangle = \langle n_{d\uparrow} \rangle - \langle n_{d\downarrow} \rangle$, starts relaxing toward the equilibrium value of zero.

In the inset panel of Fig. 3(a), we show the evolution of the logarithm of $\langle\sigma_d^z\rangle$ with different dissipation rates γ . The dynamics exhibits two stages: the first stage is a universal decrease with the total tunneling rate $\Gamma \equiv \Gamma(\omega = 0) = 4V^2/J$, which is mainly due to the single-particle tunneling of charge to the bath. The second stage for $t > 4J^{-1}$ is a linear curve, i.e., an exponential decay of $\langle\sigma_d^z\rangle$, with a rate dependent on γ , which is fitted by using $\ln\langle\sigma_d^z\rangle \sim -\Gamma_{\text{Decay}}^S t + \mathcal{C}$ with the fitting parameter Γ_{Decay}^S representing the γ -dependent relaxation rate.

We emphasize here that the evolution with $\gamma = \infty$ is unitary due to the quantum Zeno effect, hence without quantum trajectories, and it is equivalent to that of the AIM with $U_d = \infty$, in which the late-time spin relaxation is governed by the Kondo temperature $T_K \sim \sqrt{|\varepsilon_d|\Gamma} \exp(-\pi|\varepsilon_d|/\Gamma)$ [72]. As shown in the main panel of Fig. 3(a), the dynamics of the impurity magnetization slows down, in other words, Γ_{Decay}^S decreases with increasing γ . Moreover, in the high dissipation regime ($\gamma > 10^2 J$), Γ_{Decay}^S slowly converges to a small but finite value, which we will demonstrate to be the Kondo temperature. Therefore, the convergence of Γ_{Decay}^S is a clear signature of the Kondo regime. In the small dissipation regime ($\gamma \lesssim 2J$), dynamics can be treated in a mean-field (MF) approximation (cf. Appendix C), as depicted by the dotted line. The entire Γ_{Decay}^S curve represents a smooth crossover from the MF regime to the Kondo regime.

We now demonstrate that the value of Γ_{Decay}^S as $\gamma \rightarrow \infty$ in Fig. 3(a) is proportional to the Kondo temperature. We plot $\ln\Gamma_{\text{Decay}}^S$ as a function of ε_d/Γ in Fig. 3(b), which exhibits a collapse of curves with $\Gamma/J = 0.6, 1$ and $\gamma/\Gamma = 100, \infty$. This collapse shows a universal behavior of the spin relaxation rate (or the Kondo temperature) $\Gamma_{\text{Decay}}^S \sim \exp(-\eta\pi|\varepsilon_d|/\Gamma)$ with a fitting coefficient $\eta \sim 0.61$. In comparison, the renormalization group (RG) approach gives the same qualitative exponential form, but with a coefficient $\eta_{\text{RG}} = 1$ [72]. The discrepancy arises from the renormalization of the effective spin interaction between the impurity site fermions and itinerant fermions by higher-order processes in Γ/ε_d .

In summary, our approach captures the full crossover of the spin relaxation from the MF regime to the Kondo regime. In the deep Kondo regime, our approach correctly exhibits the exponential form of the spin relaxation rate Γ_{Decay}^S (or the Kondo temperature T_K).

C. Transient spin correlations

The previous analysis of the spin decay rate has focused primarily on properties of the impurity. However, the SGS approach also provides access to the correlations between the impurity and the bath. In this section, we will analyze the dynamics and quasi-stationary properties of the spin correlation functions, namely the properties of the so-called ‘‘Kondo cloud’’.

For comparison, we have performed simulations for

both the dissipative impurity model (2) and the non-dissipative AIM (3). The onsite potential of the impurity is fixed to $\varepsilon_d = -J$, and only the symmetric modes are considered. For the dissipative case, in Fig. 4(a-d) we show the spread of impurity-bath spin correlations $\langle\vec{S}_d\vec{S}_i\rangle$ starting from an initial state $|\uparrow\rangle|FS\rangle$. In accordance with physical intuition and with the Lieb-Robinson bound [73] for dissipative systems, we observe the presence of a light-cone effect, i.e., most of the correlations emerge after the passing of a wavefront propagating at a constant speed. The correlations at the wavefront are mostly ferromagnetic (FM), which can be understood as the initial magnetic moment of the impurity being carried away into the bulk of the fermionic reservoirs. Behind the first FM wavefront, correlations become mostly antiferromagnetic (AFM). We can clearly distinguish a low-dissipation ($\gamma/J = 0.1, 1$) from a high-dissipation regime ($\gamma/J = 10, 100$). In the former, the FM correlations at the wavefront decay rapidly in space and time, while a localized (non-propagating) region of AFM correlations is quickly stabilized around the impurity site. In contrast, at higher dissipation levels, the ferromagnetic correlations at the wavefront persist for an extended period, while the AFM spin correlations between the impurity and the bath gradually develop at the odd sites. The spin correlations at the even sites remain weak, with their signs shifting from negative to positive, i.e., FM. The spatially oscillating sign of impurity-bath correlations is a known property of equilibrium states of the Kondo model and AIM [74–76].

We compare the above results with the non-dissipative case of the AIM, in which double occupancies at the impurity site are suppressed by a local repulsion U_d . The result of such computation is shown in Fig. 4(f-i). We can still distinguish a weakly interacting from a strongly interacting regime, with a FM light-cone. In the former, for $U_d/J = 0.1, 1$, we also observe a FM wavefront and an AFM zone around the impurity, but compared to the dissipative case, the wavefront decays quicker and the AFM correlations are tightly localized around the impurity site—essentially concentrated on the first bath site. For large interaction strengths $U_d/J = 10, 100$, the FM wavefront is well-defined, and the correlations within the light-cone display Kondo characteristics—stronger antiferromagnetic correlations at even sites and weaker ferromagnetic correlations at odd sites. We notice that in the dissipative case, this alternating sign behavior is established only at a very strong dissipation $\gamma/J = 100$.

Finally, in Figs. 4(e) and 4(j) we compare the near-stationary properties of the impurity-bath spin correlations, evaluated at a late time $t = 20J^{-1}$. In general, we notice that the convergence to the Kondo regime $\gamma \rightarrow \infty$ or $U_d \rightarrow \infty$ (in which the two models coincide) is slower in the dissipative case than in the unitary one. When $\gamma/J = U_d/J = 1$, the correlations are AFM on all sites, but the dissipative model exhibits stronger correlations compared to the AIM. When $\gamma/J = U_d/J = 10$, while the correlations in the AIM have already acquired the

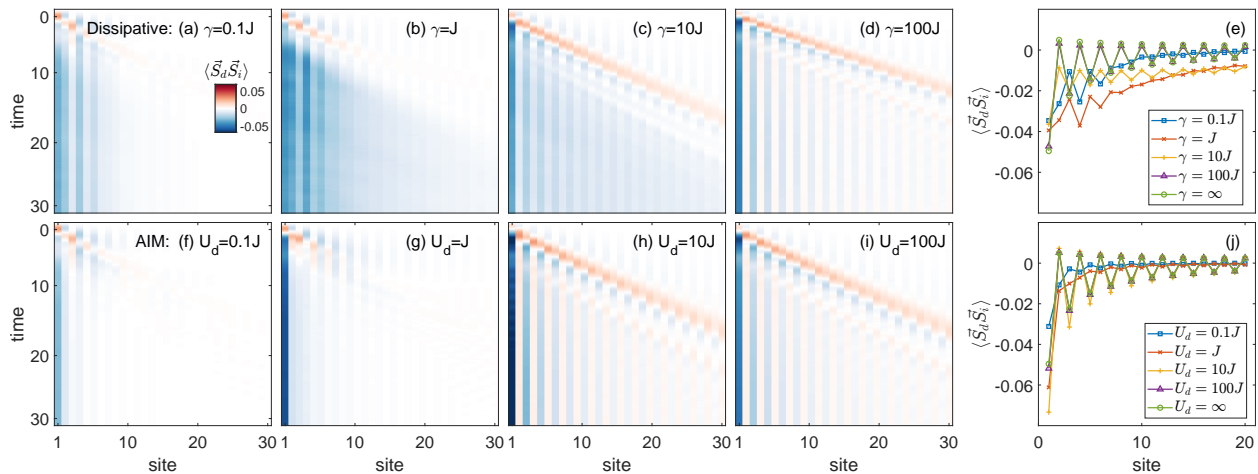


FIG. 4. Dynamic Kondo cloud of the dissipative impurity model (a-d) and non-dissipative AIM (f-i). The system is initially prepared in a product state $|\uparrow\rangle|\text{FS}\rangle$ with a system size of $\ell = 60$, after which a dissipation rate γ or repulsion coupling U_d is applied at the impurity site. The transient spin correlations between the impurity site and the bath site i (considering only symmetric modes) are computed using the SGS approach, with the time unit being J^{-1} . Panels (e) and (i) show the quasi-stationary spin correlations at time $t = 20J^{-1}$. Other parameters used are $\varepsilon_d = -J, \Gamma = 0.4J$.

alternating sign typical of the Kondo regime, in the dissipative model they are still purely AFM. Moreover, the dissipative model shows lower AFM correlations at the first site than the dissipative model. We can interpret this observation as a consequence of the fact that the two-body losses remove fermions in a spin-singlet state, so that the dissipation tends to suppress the AFM correlations (as discussed in the main text). In the Kondo regime ($\gamma/J = U_d/J = 100$) the correlation functions are quite close to each other, with both cases displaying Kondo-type spin correlations with alternating signs between even and odd sites.

Although the correlations in the dissipative model eventually reproduce those of the AIM when the loss rate and the onsite repulsion become sufficiently large, the behavior at finite dissipation is markedly different from the Hamiltonian scenario at finite U_d .

D. Charge conductance

Another signature of the Kondo regime is the enhancement in charge conductance as the system progressively enters the Kondo regime. In our setup, we measure the transport through the impurity between biased reservoirs. In the absence of dissipation, transport is suppressed by an off-resonant $\varepsilon_d < 0$, while the Kondo effect increases the conductance with a high two-body loss rate. Furthermore, transient currents and conductance can be accurately measured on recent experimental platforms, such as state-of-the-art cold-atom systems [77, 78]. Therefore, we employ next the SGS approach to investigate the charge transport of the system transitioning from the MF regime to the Kondo regime.

Considering the lattice model (23) (where we set the

charge unit to $e = 1$), the time-dependent current from the reservoir to the impurity site is given by

$$I_\alpha(t) = -\frac{dN_\alpha}{dt} = iV \sum_\sigma \text{Tr}[(d_\sigma^\dagger c_{1\sigma\alpha} - c_{1\sigma\alpha}^\dagger d_\sigma)\rho(t)], \quad (26)$$

where $N_\alpha = \sum_{i\sigma} c_{i\sigma\alpha}^\dagger c_{i\sigma\alpha}$ is the particle number of the left or right reservoir with $\alpha = L, R$. In the Kondo regime, a disentangled impurity takes a time of the order of $t_K \sim 1/T_K$ to form static antiferromagnetic correlations with the bath [74]. The real-time simulations of the dynamics are quite time-consuming as $t_K \sim \exp(\pi|\varepsilon_d|/\Gamma)$ grows exponentially with increasing $|\varepsilon_d|$. To obtain the equilibrium state efficiently, we first turn on an onsite repulsion $U_d = \gamma$ as in the AIM (3) and turn off the dissipation. By fixing $\mu_L = \mu_R = 0$, the system is then prepared in the ground state (using the imaginary time evolution in simulations [50]) of the AIM at half filling, in which a preliminary Kondo cloud is already formed. We then turn off the onsite repulsion, turn on the dissipation, and quench the chemical potentials of the bath to $\mu_{L,R} = \mp\Delta\mathcal{V}/2$ with a potential bias $\Delta\mathcal{V}$ (which plays the role of a voltage bias in usual solid-state, quantum-dot setups), while keeping the number of particles in each reservoir fixed. The combination of losses and transport generates currents, and we measure the net flow of particles from the right to the left reservoir with $I(t, \Delta\mathcal{V}) = (I_R - I_L)/2$. Note that this current does not distinguish between transported and dissipated particles. In the high dissipation regime, the transient charge conductance at zero potential bias, denoted by $G(t) = \frac{\partial I}{\partial \Delta\mathcal{V}}|_{\Delta\mathcal{V}=0}$, is anticipated to be proportional to the Kondo peak (of the impurity's spectral function) upon reaching equilibrium [79, 80]. Consequently, the conductance is strongly connected to Kondo physics and provides a signature for the Kondo regime when the im-

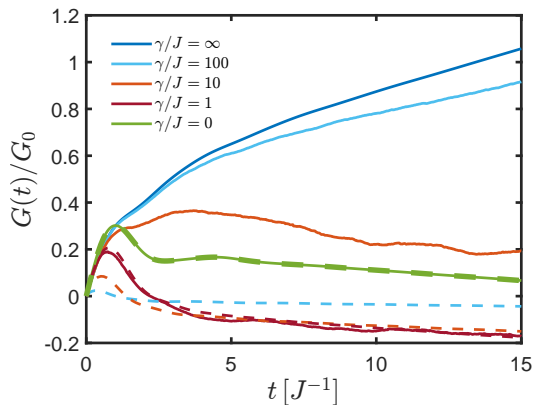


FIG. 5. Transient conductance for various dissipation rates γ . The signature of Kondo is an increase in charge conductance for transport through the impurity. We compare the SGS (solid curves) and MF (dashed curves) results, where $G_0 = 2/h$ represents the conductance quantum. In the low dissipation rate regime $\gamma \lesssim J$, the MF results agrees well with the SGS results, while the MF method fails in the high dissipation rate regime $\gamma \gtrsim 10J$. The parameters used are $\ell = 40$, $\varepsilon_d = -J$, $V = 0.5J$ and $\Delta\mathcal{V} = 0.001$.

purity potential is negative and off-resonant.

In the following, we further fix the impurity potential to $\varepsilon_d = -J$ and set the tunneling amplitude $V = 0.5J$. Fig. 5(a) presents the transient conductance with zero potential bias and different loss rates γ . For $\gamma = \infty$, the system becomes effectively closed due to the quantum Zeno effect, by which double occupations are excluded at the impurity site. The corresponding dynamics is equivalent to that of the AIM with $U_d = \infty$, which is in the Kondo regime with $\varepsilon_d < 0$. During the evolution, the conductance increases and reaches the value $G_0 = 2/h$ (after restoring the Planck constant h) at $t \simeq 15J^{-1}$. A conductance of the order of the “conductance quantum” G_0 is a signature of the Kondo regime, as it results from the emergence of the Kondo resonance near the Fermi surface [56]. At late times, we notice that the conductance tends to exceed $2/h$, which appears as a by-product of finite-size effects combined with variational errors from the SGS method [81]. For $\gamma = 100J$, the conductance curve becomes slightly lower than that of $\gamma = \infty$, indicating that residual dissipation in the strong dissipation regime leads to a small suppression of the Kondo resonance [57]. When the loss rate further decreases to $\gamma = 10J$, the conductance becomes highly suppressed with a value of $G \lesssim G_0/4$ at large times ($t \gtrsim 10J^{-1}$). Remarkably, the conductance reaches negative values when the loss rate $\gamma = J \sim \Gamma$ is intermediate. We postpone the detailed discussion of this phenomenon to Sec. V. When the loss rate decreases to $\gamma = 0$, the conductance becomes positive again with a much lower value than G_0 because the impurity potential $\varepsilon_d = -J$ is far off-resonant.

We also compare the MF results (shown as dashed lines in Fig. 5) with the SGS results. Without dissipation, both the MF and SGS approaches give the exact result.

For small dissipation rates $\gamma = J$, the MF result agrees well with the SGS result, indicating that the dynamics are approximated by one-body losses and that the spin-up and spin-down sectors of the system are nearly decoupled. For large dissipation rates $\gamma \gtrsim 10J$, the MF approximations drastically deviate from the SGS results and fail to show the increased conductance with $\gamma = 100J$ and $\gamma \rightarrow \infty$. The reason is that the entanglement between the spin-up and spin-down sectors becomes strong due to the dissipation-induced Kondo physics. However, this strong entanglement cannot be captured by MF approximations, in which the spin-up and spin-down sectors remains decoupled.

In summary, the SGS approach captures the conductance properties across all dissipation regimes. In the high dissipation regime, our approach shows conductance enhancement in the Kondo regime. In the intermediate dissipation regime, our approach reveals the exotic phenomenon of “negative conductance”.

V. ORIGIN OF “NEGATIVE CONDUCTANCE”

In this section, we analyze the “negative conductance” that appeared at intermediate dissipation rates $\gamma = J \sim \Gamma$. Since the “negative conductance” appears in the intermediate regime $\gamma \sim \Gamma$, dissipation can be effectively described by a mean-field approach in which the density matrix is assumed to be close to a Gaussian state. This ansatz approximates the original two-body loss with a self-consistent single-body loss (see Appendix C). The spin-dependent dissipation rates are given by $\gamma_\sigma = \gamma \langle n_{d\bar{\sigma}} \rangle$, where $\bar{\sigma}$ denotes the opposite spin of σ , and $\langle n_{d\bar{\sigma}} \rangle$ must be determined self-consistently. In the stationary state at late times, the self-consistency condition is

$$\langle n_{d\sigma} \rangle = -i \int \frac{d\omega}{2\pi} G_\sigma^<(\omega), \quad (27)$$

where

$$G_\sigma^<(\omega) = i \sum_\alpha f_\alpha(\omega) \Gamma_\alpha(\omega) |G_\sigma^R(\omega)|^2, \quad (28a)$$

$$G_\sigma^R(\omega) = \frac{1}{\omega - \varepsilon_d - \Sigma_L(\omega) - \Sigma_R(\omega) + \frac{i}{2}\gamma_\sigma} \quad (28b)$$

are the lesser and retarded Green functions of the impurity. Here, the self-energy for each channel is given by $\Sigma_{L,R}(\omega) = \Sigma(\omega \pm \Delta\mathcal{V}/2)$, with

$$\begin{aligned} \Sigma(\omega) &= \sum_p \frac{V_p^2}{\omega - \varepsilon_p + i0^+} \\ &= \frac{V^2}{2J} \left(\frac{\omega}{J} - \sqrt{\frac{(\omega + i0^+)^2}{J^2} - 4} \right). \end{aligned} \quad (29)$$

The latter has been calculated using the expressions (24) (with $\mu_\alpha = 0$), and quantifies the effect of the hybridization with the bath [82]. Focusing on zero temperature,

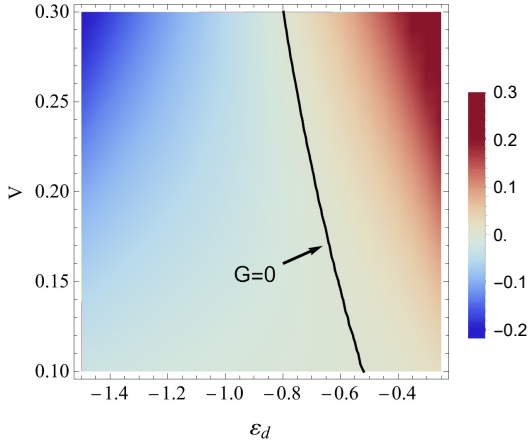


FIG. 6. Stationary conductance with the MF approximation at intermediate dissipation $\gamma = J \sim \Gamma$. The units of energy and conductance are J and $G_0 = 2/h$, respectively.

the Fermi-Dirac distribution reads $f_\alpha(\varepsilon) = \vartheta(\mp \Delta\mathcal{V}/2 - \varepsilon)$ with the Heaviside step function $\vartheta(\varepsilon)$. The tunneling rates are determined through $\Gamma_{L,R} = -2\text{Im}\Sigma_{L,R}$, whose explicit expressions are given in Eq. (25). Through the Keldysh formalism, the static current of the α -lead is given by the Meir-Wingreen formula [79]:

$$I_\alpha = \frac{i}{h} \sum_\sigma \int d\varepsilon \Gamma_\alpha(\varepsilon) [2if_\alpha(\varepsilon)\text{Im}G_\sigma^R(\varepsilon) + G_\sigma^<(\varepsilon)]. \quad (30)$$

Using Eqs. (28) and (30), the imbalanced current $I \equiv (I_R - I_L)/2 = I_{\text{ch}} + I_{\text{loss}}$ can be regarded as having two contributions [25]. The first one

$$I_{\text{ch}} = \frac{1}{h} \int d\varepsilon (f_R - f_L) \Gamma_L \Gamma_R \sum_\sigma |G_\sigma^R|^2 \quad (31)$$

receives contributions only at the edges of the band of the baths since the pre-factor $f_R - f_L$ is nonzero only at the edges. The second current

$$I_{\text{loss}} = \frac{1}{2h} \int d\varepsilon (f_R \Gamma_R - f_L \Gamma_L) \sum_\sigma \gamma_\sigma |G_\sigma^R|^2 \quad (32)$$

mostly results from the effective one-body losses of the impurity. Correspondingly, the conductance $G = G_{\text{ch}} + G_{\text{loss}}$ at zero potential bias is divided into two parts with $G_X = dI_X/d\Delta\mathcal{V}$, $X = \text{ch, loss}$. We find the main contribution to the negative G is the loss part G_{loss} . Fig. 6 shows the density plot of the total conductance G as a function of ε_d and V . The borderline of $G = 0$ (solid black curve) is near $\varepsilon_d \sim -J$, whose value of ε_d slightly increases with increasing V . The negative conductance appears in the left regime and becomes larger with increasing V and $|\varepsilon_d|$.

Physical insight into the “negative conductance” can be gained by considering a simpler case where the density of states $\Gamma_{L,R}(\varepsilon) = \Gamma$ is constant within the band $\varepsilon \in$

$[-2J \mp \Delta\mathcal{V}/2, 2J \mp \Delta\mathcal{V}/2]$. The analytic expression of the aforementioned G_{loss} then explicitly reads

$$G_{\text{loss}} = \frac{1}{2h} \sum_\sigma \left[\frac{\gamma_\sigma}{\varepsilon_d^2 + (\Gamma + \gamma_\sigma)^2} - \frac{\gamma_\sigma}{(\varepsilon_d + 2J)^2 + (\Gamma + \gamma_\sigma)^2} \right], \quad (33)$$

which clearly depends on the difference of the two band edges in Eq. (32). It is straightforward to show that $G_{\text{loss}} < 0$ if $\varepsilon_d < -J$. The physical reason is that the impurity potential $\varepsilon_d < -J$ is closer to the lower edge of the band. Therefore, the left reservoir has a larger (loss) current as a result of the one-body dissipation of the impurity.

To summarize, such “negative conductance” is a one-body phenomenon that manifests only in the presence of the aforementioned potential bias and a narrow-band scenario, in which the magnitude of the (negative) impurity potential $|\varepsilon_d|$ is comparable to (or even larger than) the bandwidth.

VI. REALIZATION OF MULTI-CHANNEL SPIN-1 KONDO PHYSICS

In this section, we discuss a simple generalization of the dissipative setup discussed so far that allows the realization of a Kondo model with spin higher than 1/2. This setup has already been briefly discussed in the companion paper [57].

A. Analytic discussion

We consider a generalized model in which the “dot” is formed by two sites of the chain, subject to two-body losses [as depicted in Fig. 7(a)]:

$$\dot{\rho} = -i[H, \rho] + \sum_{a=0,1} \frac{\gamma_a}{2} (2L_a \rho L_a^\dagger - \{L_a^\dagger L_a, \rho\}), \quad (34)$$

where

$$H = H_{\text{imp}} + H_{\text{leads}} + H_{\text{tun}}, \quad (35a)$$

$$H_{\text{imp}} = \sum_\sigma [\varepsilon_d \sum_a d_{a\sigma}^\dagger d_{a\sigma} - V(d_{0\sigma}^\dagger d_{1\sigma} + \text{H.c.})], \quad (35b)$$

$$H_{\text{leads}} = - \sum_{j\sigma\alpha} J_\alpha (c_{j\sigma\alpha}^\dagger c_{j+1\sigma\alpha} + \text{H.c.}),$$

$$H_{\text{tun}} = - \sum_{a\sigma\alpha} (\bar{J}_{a\alpha} d_{a\sigma}^\dagger c_{1\sigma\alpha} + \text{H.c.}), \quad (35c)$$

$$L_a = d_{a\uparrow} d_{a\downarrow}. \quad (35d)$$

Here, different from the lattice model (23) (with one impurity site), V and J_α denote the hopping amplitudes within the impurity sites and the bath sites, respectively. $\bar{J}_{a\alpha}$ represents the tunneling amplitudes between the impurity site a and the reservoir α . In addition, both impurity sites have two-body losses with dissipation rates γ_a , denoted by jump operators L_a . As discussed in [57], the strategy that we follow is to tune the parameters such that the dark states [83] of the set $\{H_{\text{imp}}, L_0, L_1\}$ —which would be stationary in the absence of the leads—form a low-energy spin-1 multiplet. In the case of Eq. (35), the dark subspace consists of four sets of states: the empty impurity state $|\mathcal{N}=0, \mathcal{S}=0, \mathcal{M}=0\rangle$ with zero energy, two doublets $|\pm, \mathcal{N}=1, \mathcal{S}=1/2, \mathcal{M}\rangle$ with energy $\varepsilon_d \mp V$ and a triplet $|\mathcal{N}=2, \mathcal{S}=1, \mathcal{M}\rangle$ with energy $2\varepsilon_d$, where \mathcal{N} and \mathcal{S} denote the particle number and the total spin, respectively, and the magnetization takes the values $\mathcal{M} = -\mathcal{S}, \dots, \mathcal{S}$. As noted in [57], the bright states (i.e. the ones outside of the dark subspace) of the dissipative, two-site dot have nontrivial properties—in particular, the slowest decay rate γ_{min} of the bright states is non-monotonic in γ (with fixed V), and goes to zero both for $\gamma \rightarrow 0$ and $\gamma \rightarrow +\infty$. Therefore, to ensure that dissipation suppresses the population of all states except the dark subspace, one needs to work close to the maximal value of $\gamma_{\text{min}} \propto \gamma$, which occurs for $\gamma \propto V$. Summarizing, if we have

$$\gamma \sim V \sim |\varepsilon_d|, \quad (36a)$$

$$\Delta\varepsilon = -\varepsilon_d - V > 0, \quad (36b)$$

then for times larger than a few γ^{-1} the dynamics will be confined to the dark subspace [84]. The second condition (36b) ensures that the lower spin-1/2 doublet has a higher energy than the spin-1 triplet. Since we are interested in the limit $V \sim \gamma \rightarrow +\infty$, we also need to require $|\varepsilon_d| \sim V$ to keep $\Delta\varepsilon$ finite and allow particle exchanges with the leads. In the spirit of adiabatic elimination [85, 86], to the lowest order in γ^{-1} , the effective dynamics of the system will be projected onto the dark subspace, even after turning on the tunneling \bar{J} with the leads. This construction leads to an effective Hamiltonian dynamics governed by an ionic model [56, 87, 88]. If the coupling to the leads is sufficiently weak,

$$|\Delta\varepsilon| \gg \Gamma \sim \frac{\bar{J}^2}{J}, \quad (37)$$

the effective model can be mapped via a *unitary* Schrieffer-Wolff transformation to a spin-1 Kondo model:

$$H_{S=1} = \sum_{\alpha\beta} \frac{\tilde{J}_\alpha \tilde{J}_\beta}{2|\Delta\varepsilon|} \tilde{S}_{\text{imp}} \vec{s}_{\alpha\beta} + H_{\text{leads}}. \quad (38)$$

In the expression above, we have introduced the $SU(2)$ impurity spin \tilde{S}_{imp} belonging to the spin-1 representation and the bath spin-1/2 operators $s_{\alpha\beta}^{x,y,z} =$

$\frac{1}{2} c_{1\sigma\alpha}^\dagger \tau_{\sigma\sigma'}^{x,y,z} c_{1\sigma'\beta}$. The notation $\tilde{J}_\alpha = \sum_a (-1)^a f_a \bar{J}_{a\alpha}$, with $f_0 = 1$, $f_1 = \text{sign}(V) = \pm 1$, corresponds to the ground-state wave functions of H_{imp} in the one-particle sector. Note that if V is positive and the hopping amplitudes $\bar{J}_{a\sigma}$ are the same, all \tilde{J}_α become zero due to the parity, and the effective Hamiltonian (38) thus vanishes. Physically [56, 72], Eq. (38) describes a situation where the low-lying spin triplet state is always occupied (i.e. the impurity is always hosting two fermions) and behaves like a spin 1 object, while the lead-mediated transitions to the spin-1/2 states are virtual, and cause an antiferromagnetic interaction between \tilde{S}_{imp} and the lead fermions. We observe that, with the same tuning of the loss rate and hopping as above, but with $\Delta\varepsilon < 0$, we can map the effective, strong-dissipation dynamics to a spin-1/2 Kondo model:

$$H_{S=1/2} = \sum_{\alpha\beta ab} \frac{\tilde{J}_{\alpha a} \tilde{J}_{\beta b}}{2\sqrt{2}|\Delta\varepsilon|} \vec{S}_{\text{imp}} \vec{s}_{\alpha\beta} + H_{\text{leads}}, \quad (39)$$

where $\vec{S}_{\text{imp}}^2 = 3/4$.

It is easy to see that the coupling to the leads will generally endow the dark states of H_{imp} with a finite lifetime, an effect that is captured by the first-order terms in the dissipative Schrieffer-Wolff transformation, analogous with the scenario of a single dissipative site. While we will not pursue this calculation here, it is straightforward to estimate that the spin-1 states will suffer from a decay rate of order \bar{J}^2/γ , since they are coupled to the bright states by the tunneling of a single fermion from the leads. Drawing on the results of [57] for the single-site case, we can then expect that the competition between the emerging Kondo physics and the residual dissipation will allow observation of the former as long as

$$\frac{\bar{J}^2}{\gamma} \lesssim T_K \sim \sqrt{\Gamma|\Delta\varepsilon|} e^{-\pi \frac{|\Delta\varepsilon|}{\Gamma}}, \quad (40)$$

where T_K is the Kondo temperature. It is interesting to note that the spin-1/2 dark states are connected to the bright states by two tunneling events, hence they will have a suppressed decay rate \bar{J}^4/γ . Therefore, in the case of $\Delta\varepsilon < 0$, the effective Hamiltonian (39) would be more protected from the residual dissipation.

B. Stability of impurity ferromagnetism

In the previous section, we delineated a possible mapping from a model with two dissipative sites to a spin-1 Kondo model. Essentially, this mapping relies on the ability of two-body losses to stabilize a ferromagnetic (FM) region on the impurity sites. The triplet of spin-1 states mentioned before represent precisely these kind of states. More generally, a FM behavior is generically expected from two-body losses even in longer dissipative chains [71].

In this Section, we corroborate the existence of FM intra-dot correlations in the model (35) of two strongly

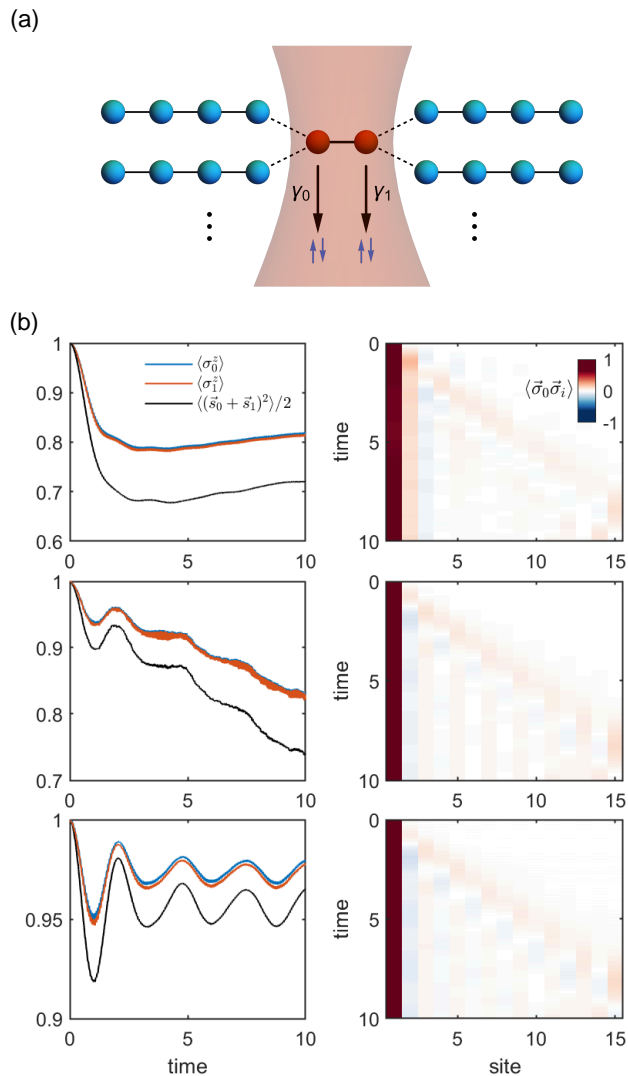


FIG. 7. (a) Schematic depiction of the generalized model, with two impurity sites undergoing two-body losses. (b) Stabilization of a ferromagnetic impurity, observed through SGS simulations. The right panel shows the transient spin correlations $\langle \vec{\sigma}_0 \vec{\sigma}_i \rangle$ with $\gamma = 0, V, \infty$ (from top to bottom) and the initial state $|\uparrow\uparrow\rangle_d |\text{FS}\rangle_l$. The time unit is J^{-1} and the parameters used are $V = 50J, \Delta\varepsilon = 2J, \ell = 15$. The FM domain is stabilized by large dissipation.

coupled impurity sites, in which only one is subjected to two-body losses $\gamma_0 = \gamma, \gamma_1 = 0$ while the other is connected to a single lead. To probe the stability of impurity ferromagnetism, we have run our SGS simulations with the initial state $|\uparrow\uparrow\rangle_d |\text{FS}\rangle_l$, where $|\uparrow\uparrow\rangle_d = d_{0\uparrow}^\dagger d_{1\uparrow}^\dagger |0\rangle_d$ is an initial, spin-polarized impurity state and $|\text{FS}\rangle_l$ is a half-filled Fermi sea of the lead with zero net magnetization. In Fig. 7(b) we show the results of the SGS calculations with increasing dissipation $\gamma = 0, V, \infty$ and for strongly coupled impurity sites $V = 50J$. The onsite energies ε_d are chosen such that $\Delta\varepsilon = 2J$ is smaller than the bandwidth of the lead, thus allowing for resonant ex-

changes of particles. The left panels of the Figure show the time evolution of the average spin orientations $\langle \sigma_0^z \rangle$ and $\langle \sigma_1^z \rangle$ at the two impurity sites, and the magnitude $\langle \vec{S}_{\text{imp}}^2 \rangle$ of the total spin, $\vec{S}_{\text{imp}} = \vec{s}_0 + \vec{s}_1$. The overall magnitude of $\langle \sigma_{0,1}^z \rangle$ decreases in time for both $\gamma = 0$ and $\gamma = V$, albeit in quite different ways—most recognizably, the behavior in the former case is not monotonic. For $\gamma = \infty$, the dynamics of $\langle \sigma_{0,1}^z \rangle$ is nearly “frozen”, namely both spins fluctuate only slightly with respect to their initial value. The behavior of the total impurity spin magnitude $\langle \vec{S}_{\text{imp}}^2 \rangle$ mirrors the local magnetizations: it decays significantly for $\gamma = 0$ and V , while it oscillates around 1.9 for $\gamma \rightarrow \infty$ —quite close to the perfect spin-1 value $\langle \vec{S}_{\text{imp}}^2 \rangle = 2$. Thus, we observe that the combination of a strong coupling V between the impurity sites and dissipation enforces a collective dynamics of the total impurity spin.

The right panels of Fig. 7(b) show the spin correlations $\langle \vec{\sigma}_0 \vec{\sigma}_i \rangle$ between the dissipative site $i = 0$ and the other sites, i.e. the second impurity site $i = 1$ and the lead sites $i \geq 2$. These plots confirm the establishment of a strong FM correlation between the two impurity sites, which is further stabilized by increasing γ . The correlations in the rest of the system are far weaker, and emerge after the passage of a slightly FM light-cone. Notably, the correlations with the lead sites $i > 1$ exhibit alternating signs for $\gamma > 0$, starting with an AFM correlation for $i = 2$, while for $\gamma = 0$ there is a small “leakage” of FM correlations to the first bath site.

Summing up, these preliminary simulations confirm the picture we presented in the previous section—that is, two impurity sites can be tuned to behave like a spin-1 impurity by suitably choosing their energies, tunneling rates, and dissipation. With the present choice of parameters, a very large loss rate γ appears to be the most suitable setup for obtaining an effective spin-1, as it gives a value of $\langle \vec{S}_{\text{imp}}^2 \rangle$ closer to 2. This conclusion might seem at odds with the the previous section (cf. also [57]), where we mentioned that for $\gamma \rightarrow +\infty$ the dark subspace includes also other non-FM states besides the Dicke multiplets. However, for the large value of V chosen in this section, these states are extremely off-resonant with respect to the transitions with the bath and thus can be considered to be excluded from the dynamics.

VII. CONCLUSIONS AND OUTLOOK

In this work, we introduced a non-perturbative framework that combines the SGS variational ansatz with the quantum trajectory approach, offering an efficient method for simulating dissipative impurity systems. We applied this method to a system where a spinful impurity, subject to two-body losses, interacts with a bath of non-interacting fermions. Through this approach, we demonstrated that strong localized two-body losses can induce the Kondo effect, consistent with findings in related re-

search [57]. The key signatures of Kondo physics, such as the slowdown of spin relaxation and the enhancement of charge conductance, were effectively captured using the SGS framework. This method allowed us to thoroughly examine the full crossover from the weakly correlated mean-field regime at small dissipation to the strongly correlated Kondo regime at large dissipation, thereby providing a comprehensive understanding of the system's behavior across different dissipation regimes. Notably, in the mean-field regime, we revealed the emergence of exotic “reverse conductance” at zero potential bias, which arises from intermediate dissipation and the constraints of a finite reservoir bandwidth.

Our framework can be extended to more complex scenarios, including systems with multiple dissipative impurity sites or involving a superconducting or Mott-like fermionic baths. Our exploration of dissipative Kondo models suggests new directions for utilizing localized dissipation to potentially realize large-scale, tunable spin-1/2 and higher-spin Kondo systems in cold-atom setups. These systems could serve as a basis for investigating strongly correlated phenomena within the broader Kondo problem family, such as quantum criticality [89–97], fractionalization [98–104], and multistage Kondo effects [105–110].

VIII. ACKNOWLEDGMENTS

We acknowledge useful discussions with W. Zhang, D. Sels, A. Gomez Salvador, R. Andrei, M. Kiselev, Y.Q. and E.D. acknowledge support by the SNSF project 200021_212899, NCCR SPIN, a National Centre of Competence in Research, funded by the Swiss National Science Foundation (grant number 225153), the Swiss State Secretariat for Education, Research and Innovation (contract number UeM019-1). E.D. also acknowledges support from the ARO grant number W911NF-20-1-0163. T.E., Y.Q., and E.D. acknowledge funding by the ETH grant. M.S. and J.M. have been supported by the DFG through the grant HADEQUAM-MA7003/3-1. J.M. acknowledges the Pauli Center for hospitality. The numerical simulations were performed on the ETH Euler cluster.

Appendix A: Calculation of $\bar{c}|\text{GS}_s\rangle$ and $\bar{c}^\dagger|\text{GS}_s\rangle$

In this appendix, we provide analytical details on Eq. (16)—namely, on how to calculate $\bar{c}|\text{GS}_s\rangle$ and $\bar{c}^\dagger|\text{GS}_s\rangle$ given the Gaussian state $|\text{GS}_s\rangle$ and $\bar{c}^\dagger = \sum_{j=1}^{N_f} v_j C_j^\dagger$. We recall that the Gaussian state is expressed as a single Slater determinant, given by $|\text{GS}_s\rangle = \bar{C}_1^\dagger \bar{C}_2^\dagger \dots \bar{C}_{N_s}^\dagger |0\rangle$. Here, the operators $\bar{C}_i^\dagger = \sum_{j=1}^{N_f} u_{ij} C_j^\dagger$, where $i = 1, \dots, N_s$ represent the occupied modes, and the $N_f \times N_s$ matrix u contains the associated wavefunctions.

To calculate $\bar{c}^\dagger|\text{GS}_s\rangle$, we decompose the creation op-

erator \bar{c}^\dagger as follows:

$$\bar{c}^\dagger = \beta \tilde{c}^\dagger + \sum_{i=1}^{N_s} f_i \bar{C}_i^\dagger. \quad (\text{A1})$$

Here, the first term represents a normalized mode $\tilde{c}^\dagger = \sum_{j=1}^{N_f} \tilde{v}_j C_j^\dagger$, where $\tilde{\mathbf{v}} = (\mathbf{v} - uu^\dagger \mathbf{v})/\beta$ that is orthogonal to the occupied modes of $|\text{GS}_s\rangle$, and is weighted by $\beta = \|\mathbf{v} - uu^\dagger \mathbf{v}\|$. In the previous expressions, \mathbf{v} is the vector collecting the coefficients v_j . The second term is a linear combination of the occupied modes with coefficients $f_i = \sum_{j=1}^{N_f} u_{ij}^* v_j$, which annihilates $\bar{c}^\dagger|\text{GS}_s\rangle$ due to the Pauli exclusion principle. Therefore, $\bar{c}^\dagger|\text{GS}_s\rangle$ simplifies to:

$$\bar{c}^\dagger|\text{GS}_s\rangle = \beta \tilde{c}^\dagger \bar{C}_1^\dagger \bar{C}_2^\dagger \dots \bar{C}_{N_s}^\dagger |0\rangle \equiv \beta |\widetilde{\text{GS}}_s\rangle. \quad (\text{A2})$$

The last equality defines a new Slater determinant and hence a new Gaussian state.

Next, to calculate $\bar{c}|\text{GS}_s\rangle$, we notice that only the second term in Eq. (A1) contributes, as it represents a superposition of the occupied modes. We recombine the occupied modes into $\bar{C}'_i = \sum_{i'=1}^{N_s} \omega_{ii'} \bar{C}'_{i'}$, $i = 1, \dots, N_s$, where ω is a unitary $N_s \times N_s$ matrix whose first column is $\mathbf{f}/\|\mathbf{f}\|$ (\mathbf{f} is the vector of the coefficients f_j defined in the previous paragraph) and the remaining columns are orthogonal to \mathbf{f} . The ambiguity in the definition of ω is harmless, since it will correspond to the choice of the overall phase of $\bar{c}|\text{GS}_s\rangle$. In terms of the new modes \bar{C}'_i , the Gaussian state can be expressed as $|\text{GS}_s\rangle = \det(\omega)^{-1} \bar{C}'_1 \bar{C}'_2 \dots \bar{C}'_{N_s} |0\rangle$ and $\bar{c} = \beta \tilde{c} + \|\mathbf{f}\| \bar{C}'_1$, from which we see that the operator \bar{c} simply removes the first mode \bar{C}'_1 from the state $|\text{GS}_s\rangle$. Therefore, we obtain

$$\bar{c}|\text{GS}_s\rangle = \beta' \bar{C}'_2 \dots \bar{C}'_{N_s} |0\rangle \equiv \beta' |\widetilde{\text{GS}}'_s\rangle, \quad (\text{A3})$$

which defines a new Gaussian state, with the coefficient $\beta' = \|\mathbf{f}\|/\det(\omega)$.

Appendix B: Evolution of the state after a quantum jump

In this appendix, we describe the procedure for determining the evolution of the quantum state immediately following a quantum jump. The simple projection rules (22) leave the bath's Gaussian states corresponding to the singly and doubly occupied impurity undefined. We will show how to resolve this ambiguity by performing a short-time evolution of the post-jump state under the non-Hermitian Hamiltonian H_{NH} .

Assume a quantum jump occurs at time t_1 in a quantum trajectory. Immediately after the jump, the state of the trajectory is given by $|\Psi(t_1^+)\rangle = |0\rangle|\text{GS}_0\rangle$, where the Gaussian state $|\text{GS}_0\rangle$ can be represented by the unitary matrix $U_0(t_1^+) = U_2(t_1^-)$, as described in Sec. III C. Our task is to obtain the new matrices $U_{\uparrow,\downarrow,2}(t_1^+)$ after the jump. We evolve the state $|\Psi(t_1^+)\rangle$ for a small time

interval δt under the non-Hermitian Hamiltonian H_{NH} , using a Taylor expansion:

$$\begin{aligned} |\Psi(t_1 + \delta t)\rangle &= \exp(-iH_{\text{NH}}\delta t) |\Psi(t_1^+)\rangle \\ &= [1 - iH_{\text{NH}}\delta t - \frac{1}{2}H_{\text{NH}}^2\delta t^2 + o(\delta t^2)] |0\rangle |\text{GS}_0\rangle \\ &\approx |0\rangle |\text{GS}_0\rangle + \sum_{s'=\uparrow,\downarrow,2} \alpha_{s'} |s'\rangle |\text{GS}_{s'}\rangle. \end{aligned} \quad (\text{B1})$$

Since the action of H_{NH} can transfer at most one fermion from the reservoirs to the impurity, we need to keep terms up to the second order to recover all four impurity states. By retaining the leading term for each impurity subsector, we can represent $|\Psi(t_1 + \delta t)\rangle$ as a SGS in the third line of Eq. (B1). The Gaussian states and their coefficients are given by

$$\begin{aligned} \alpha_\uparrow |\text{GS}_\uparrow\rangle &= -i\delta t \bar{c}_\uparrow |\text{GS}_0\rangle, \\ \alpha_\downarrow |\text{GS}_\downarrow\rangle &= i\delta t \bar{c}_\downarrow |\text{GS}_0\rangle, \\ \alpha_2 |\text{GS}_2\rangle &= \delta t^2 \bar{c}_\uparrow \bar{c}_\downarrow |\text{GS}_0\rangle, \end{aligned} \quad (\text{B2})$$

which can be calculated using Eq. (A3). The first $N_{s'}$ (representing the number of bath particles in the impurity subsector s') columns of the corresponding matrix $U_{s'}$ are determined by the wavefunctions of the occupied modes in $|\text{GS}_{s'}\rangle$. The remaining columns of $U_{s'}$ are chosen to be orthonormal to the first $N_{s'}$ columns. The updated SGS, as described in Eq. (B1), is then used to continue the simulation of real-time evolutions through the SGS approach, utilizing the variational parameters α_s and U_s .

Appendix C: Gaussian state approach

In this appendix, we present the Gaussian state (GS) approach [64], a self-consistent mean-field method, applied to the dissipative impurity model described by Eq. (2).

As stated in the main text, we approximate the density matrix of the system with a Gaussian density matrix ρ_{GS} , which is fully characterized by the correlation matrix $\varrho_{ij} = \text{Tr}(\rho_{\text{GS}} c_i^\dagger c_j)$. The spin index is absorbed into

i and j for simplicity. Considering the master equation (1), the EoM of the correlation matrix are given by

$$\begin{aligned} \frac{d}{dt} \varrho_{ij} &= \langle i[H, c_i^\dagger c_j] - \frac{\gamma}{2} \{L^\dagger L, c_i^\dagger c_j\} + \gamma L^\dagger c_i^\dagger c_j L \rangle \\ &= -i \sum_k \langle c_i^\dagger h_{jk} c_k - c_k^\dagger h_{ki} c_j \rangle \\ &\quad - \frac{\gamma}{2} \langle \sum_k l_{jk} c_i^\dagger c_k + l_{ki} c_k^\dagger c_j \rangle, \end{aligned} \quad (\text{C1})$$

where $\langle \dots \rangle = \text{Tr}(\rho_{\text{GS}} \dots)$ represents the expectation value and the Wick contraction theorem has been applied in the second equality. Since particle number is conserved, we focus exclusively on the Hartree-Fock contributions, i.e. we have discarded any anomalous correlation $\langle c_i c_j \rangle$ or $\langle c_i^\dagger c_j^\dagger \rangle$. The Hermitian matrices h and l are derived by expressing $H = C^\dagger h C$ and $L^\dagger L = C^\dagger l C$, where $C = (c_1, c_2, c_3, \dots)^T$ denotes a column vector composed of the annihilation operators.

It can be shown that the EoM (C1) corresponds to an effective master equation involving one-body losses at the impurity site

$$\dot{\rho}_{\text{GS}}(t) = -i[H, \rho_{\text{GS}}] + \mathcal{L}_{\text{GS}} \rho_{\text{GS}}, \quad (\text{C2})$$

with a one-body dissipation term:

$$\mathcal{L}_{\text{GS}} \rho_{\text{GS}} = \sum_{\sigma\sigma'=\uparrow,\downarrow} \gamma_{\sigma\sigma'}(t) (c_{0\sigma} \rho_{\text{GS}} c_{0\sigma'}^\dagger - \frac{1}{2} \{c_{0\sigma'}^\dagger c_{0\sigma}, \rho_{\text{GS}}\}), \quad (\text{C3})$$

in which the one-body loss rates $\gamma_{\sigma\sigma'}(t) = \gamma \text{Tr}[\rho(t) c_{0\sigma'}^\dagger c_{0\sigma}]$ depend self-consistently on the correlation functions at the impurity sites.

The effective master equation has the property that if the initial density matrix is a product state of the spin-up and spin-down sectors, such that $\rho(t=0) = \rho_\uparrow \rho_\downarrow$, this property will be conserved during the dynamics. Hence, the correlations $\varrho_{j\uparrow, j'\downarrow} = 0$ will vanish throughout the evolution and we will have $\gamma_{\sigma\sigma'} = \delta_{\sigma\sigma'} \gamma n_{0\bar{\sigma}}(t)$. However, the Kondo effect at large dissipation implies that the true dynamics will generate a non-negligible entanglement between the two spin sectors. Hence, the GS approach cannot be valid beyond a moderate dissipation rate $\gamma \sim \Gamma$.

-
- [1] A. J. Leggett, S. Chakravarty, A. T. Dorsey, M. P. A. Fisher, A. Garg, and W. Zwerger, Dynamics of the dissipative two-state system, *Rev. Mod. Phys.* **59**, 1 (1987).
 - [2] B. Kraus, H. P. Büchler, S. Diehl, A. Kantian, A. Micheli, and P. Zoller, Preparation of entangled states by quantum Markov processes, *Phys. Rev. A* **78**, 042307 (2008).
 - [3] S. Diehl, A. Micheli, A. Kantian, B. Kraus, H. Büchler, and P. Zoller, Quantum states and phases in driven open quantum systems with cold atoms, *Nature Physics* **4**,

- 878 (2008).
- [4] F. Verstraete, M. M. Wolf, and J. Ignacio Cirac, Quantum computation and quantum-state engineering driven by dissipation, *Nature physics* **5**, 633 (2009).
- [5] Y. Lin, J. Gaebler, F. Reiter, T. R. Tan, R. Bowler, A. Sørensen, D. Leibfried, and D. J. Wineland, Dissipative production of a maximally entangled steady state of two quantum bits, *Nature* **504**, 415 (2013).
- [6] C.-E. Bardyn, M. A. Baranov, C. V. Kraus, E. Rico, A. İmamoğlu, P. Zoller, and S. Diehl, Topology by dis-

- sipation, *New Journal of Physics* **15**, 085001 (2013).
- [7] S. Shankar, M. Hatridge, Z. Leghtas, K. Sliwa, A. Narla, U. Vool, S. M. Girvin, L. Frunzio, M. Mirrahimi, and M. H. Devoret, Autonomously stabilized entanglement between two superconducting quantum bits, *Nature* **504**, 419 (2013).
- [8] M. Nakagawa, N. Tsuji, N. Kawakami, and M. Ueda, Dynamical sign reversal of magnetic correlations in dissipative Hubbard models, *Phys. Rev. Lett.* **124**, 147203 (2020).
- [9] M. Raghunandan, F. Wolf, C. Ospelkaus, P. O. Schmidt, and H. Weimer, Initialization of quantum simulators by sympathetic cooling, *Science Advances* **6**, eaaw9268 (2020).
- [10] L. M. Sieberer, M. Buchhold, J. Marino, and S. Diehl, *Universality in driven open quantum matter* (2023), [arXiv:2312.03073](https://arxiv.org/abs/2312.03073) [[cond-mat.stat-mech](https://arxiv.org/abs/2312.03073)].
- [11] R. Ma, B. Saxberg, C. Owens, N. Leung, Y. Lu, J. Simon, and D. I. Schuster, A dissipatively stabilized mott insulator of photons, *Nature* **566**, 51 (2019).
- [12] X. Mi, *et al.*, Stable quantum-correlated many-body states through engineered dissipation, *Science* **383**, 1332 (2024).
- [13] E. G. Dalla Torre, E. Demler, T. Giamarchi, and E. Altman, Quantum critical states and phase transitions in the presence of non-equilibrium noise, *Nature Physics* **6**, 806 (2010).
- [14] E. G. Dalla Torre, E. Demler, T. Giamarchi, and E. Altman, Dynamics and universality in noise-driven dissipative systems, *Phys. Rev. B* **85**, 184302 (2012).
- [15] B. Misra and E. C. G. Sudarshan, The Zeno's paradox in quantum theory, *Journal of Mathematical Physics* **18**, 756 (1977).
- [16] M. C. Fischer, B. Gutiérrez-Medina, and M. G. Raizen, Observation of the quantum Zeno and anti-Zeno effects in an unstable system, *Phys. Rev. Lett.* **87**, 040402 (2001).
- [17] P. Facchi and S. Pascazio, Quantum Zeno subspaces, *Phys. Rev. Lett.* **89**, 080401 (2002).
- [18] N. Syassen, D. M. Bauer, M. Lettner, T. Volz, D. Dietze, J. J. García-Ripoll, J. I. Cirac, G. Rempe, and S. Dürr, Strong dissipation inhibits losses and induces correlations in cold molecular gases, *Science* **320**, 1329 (2008).
- [19] P. Facchi and S. Pascazio, Quantum Zeno dynamics: mathematical and physical aspects, *Journal of Physics A: Mathematical and Theoretical* **41**, 493001 (2008).
- [20] Y. Sun, T. Shi, Z. Liu, Z. Zhang, L. Xiao, S. Jia, and Y. Hu, Fractional quantum Zeno effect emerging from non-hermitian physics, *Phys. Rev. X* **13**, 031009 (2023).
- [21] L. M. Sieberer, S. D. Huber, E. Altman, and S. Diehl, Dynamical critical phenomena in driven-dissipative systems, *Phys. Rev. Lett.* **110**, 195301 (2013).
- [22] E. G. D. Torre, S. Diehl, M. D. Lukin, S. Sachdev, and P. Strack, Keldysh approach for nonequilibrium phase transitions in quantum optics: Beyond the Dicke model in optical cavities, *Physical Review A—Atomic, Molecular, and Optical Physics* **87**, 023831 (2013).
- [23] L. M. Sieberer, M. Buchhold, and S. Diehl, Keldysh field theory for driven open quantum systems, *Reports on Progress in Physics* **79**, 096001 (2016).
- [24] M. F. Maghrebi and A. V. Gorshkov, Nonequilibrium many-body steady states via Keldysh formalism, *Phys. Rev. B* **93**, 014307 (2016).
- [25] M. Gievers, T. Müller, H. Fröml, S. Diehl, and A. Chiochetta, *Transport manifestations of fluctuation-induced effects in dissipative impurities* (2023), [arXiv:2312.12656](https://arxiv.org/abs/2312.12656).
- [26] Z. Cai and T. Barthel, Algebraic versus exponential decoherence in dissipative many-particle systems, *Phys. Rev. Lett.* **111**, 150403 (2013).
- [27] M. Žnidarič, Relaxation times of dissipative many-body quantum systems, *Phys. Rev. E* **92**, 042143 (2015).
- [28] A. J. Daley, J. M. Taylor, S. Diehl, M. Baranov, and P. Zoller, Atomic three-body loss as a dynamical three-body interaction, *Phys. Rev. Lett.* **102**, 040402 (2009).
- [29] L. Bonnes and A. M. Läuchli, *Superoperators vs. trajectories for matrix product state simulations of open quantum system: A case study* (2014), [arXiv:1411.4831](https://arxiv.org/abs/1411.4831) [[cond-mat.quant-gas](https://arxiv.org/abs/1411.4831)].
- [30] K. Yamamoto, M. Nakagawa, M. Tezuka, M. Ueda, and N. Kawakami, Universal properties of dissipative Tomonaga-Luttinger liquids: Case study of a non-hermitian xxz spin chain, *Phys. Rev. B* **105**, 205125 (2022).
- [31] E. Mascarenhas, H. Flayac, and V. Savona, Matrix-product-operator approach to the nonequilibrium steady state of driven-dissipative quantum arrays, *Phys. Rev. A* **92**, 022116 (2015).
- [32] J. Cui, J. I. Cirac, and M. C. Bañuls, Variational matrix product operators for the steady state of dissipative quantum systems, *Phys. Rev. Lett.* **114**, 220601 (2015).
- [33] B. Buča, C. Booker, M. Medenjak, and D. Jaksch, Bethe ansatz approach for dissipation: exact solutions of quantum many-body dynamics under loss, *New Journal of Physics* **22**, 123040 (2020).
- [34] M. Nakagawa, N. Kawakami, and M. Ueda, Exact liouvilian spectrum of a one-dimensional dissipative Hubbard model, *Phys. Rev. Lett.* **126**, 110404 (2021).
- [35] V. Alba, *Free fermions with dephasing and boundary driving: Bethe ansatz results* (2023), [arXiv:2309.12978](https://arxiv.org/abs/2309.12978).
- [36] C. Ekman and E. J. Bergholtz, *Liouvillian skin effects and fragmented condensates in an integrable dissipative Bose-Hubbard model* (2024), [arXiv:2402.10261](https://arxiv.org/abs/2402.10261).
- [37] M. J. Hartmann and G. Carleo, Neural-network approach to dissipative quantum many-body dynamics, *Physical review letters* **122**, 250502 (2019).
- [38] L. J. Bond, B. Gerritsen, J. Minář, J. T. Young, J. Schachenmayer, and A. Safavi-Naini, *Open quantum dynamics with variational non-Gaussian states and the truncated Wigner approximation* (2024), [arXiv:2407.02617](https://arxiv.org/abs/2407.02617) [[quant-ph](https://arxiv.org/abs/2407.02617)].
- [39] F. Tonielli, R. Fazio, S. Diehl, and J. Marino, Orthogonality catastrophe in dissipative quantum many-body systems, *Phys. Rev. Lett.* **122**, 040604 (2019).
- [40] M. Will, J. Marino, H. Ott, and M. Fleischhauer, Controlling superfluid flows using dissipative impurities, *SciPost Phys.* **14**, 064 (2023).
- [41] P. E. Dolgirev, J. Marino, D. Sels, and E. Demler, Non-Gaussian correlations imprinted by local dephasing in fermionic wires, *Phys. Rev. B* **102**, 100301(R) (2020).
- [42] F. Tonielli, N. Chakraborty, F. Grusdt, and J. Marino, Ramsey interferometry of non-Hermitian quantum impurities, *Phys. Rev. Res.* **2**, 032003(R) (2020).
- [43] A. P. Chaudhari, S. P. Kelly, R. J. Valencia-Tortora, and J. Marino, Zeno crossovers in the entanglement speed of spin chains with noisy impurities, *Journal of Statistical Mechanics: Theory and Experiment* **2022**, 103101

- (2022).
- [44] J. Kondo, Resistance Minimum in Dilute Magnetic Alloys, *Progress of Theoretical Physics* **32**, 37 (1964).
- [45] P. W. Anderson, Localized magnetic states in metals, *Phys. Rev.* **124**, 41 (1961).
- [46] L. D. Landau, 10 - electron motion in crystal lattices, in *Collected Papers of L.D. Landau*, edited by D. TER HAAR (Pergamon, 1965) pp. 67–68.
- [47] S. Pekar, Local quantum states of electrons in an ideal ion crystal, *Zhurnal Eksperimentalnoi I Teoreticheskoi Fiziki* **16**, 341 (1946).
- [48] S. Bravyi and D. Gosset, Complexity of quantum impurity problems, *Communications in Mathematical Physics* **356**, 451 (2017).
- [49] S. Boutin and B. Bauer, Quantum impurity models using superpositions of fermionic Gaussian states: Practical methods and applications, *Phys. Rev. Res.* **3**, 033188 (2021).
- [50] W. Zhang and T. Shi, in preparation.
- [51] J. Dalibard, Y. Castin, and K. Mølmer, Wave-function approach to dissipative processes in quantum optics, *Phys. Rev. Lett.* **68**, 580 (1992).
- [52] K. Mølmer, Y. Castin, and J. Dalibard, Monte Carlo wave-function method in quantum optics, *J. Opt. Soc. Am. B* **10**, 524 (1993).
- [53] R. Dum, P. Zoller, and H. Ritsch, Monte Carlo simulation of the atomic master equation for spontaneous emission, *Phys. Rev. A* **45**, 4879 (1992).
- [54] R. Dum, A. S. Parkins, P. Zoller, and C. W. Gardiner, Monte Carlo simulation of master equations in quantum optics for vacuum, thermal, and squeezed reservoirs, *Phys. Rev. A* **46**, 4382 (1992).
- [55] H. Carmichael, *An Open Systems Approach to Quantum Optics: Lectures Presented at the Université Libre de Bruxelles, October 28 to November 4, 1991*, Lecture Notes in Physics New Series M, Monographs No. 18 (Springer).
- [56] A. C. Hewson, *The Kondo Problem to Heavy Fermions*, Cambridge Studies in Magnetism (Cambridge University Press, 1993).
- [57] M. Stefanini, Y.-F. Qu, T. Esslinger, S. Gopalakrishnan, E. Demler, and J. Marino, *Dissipative realization of Kondo models*, arXiv:2406.03527.
- [58] B. Yan, S. A. Moses, B. Gadway, J. P. Covey, K. R. A. Hazzard, A. M. Rey, D. S. Jin, and J. Ye, Observation of dipolar spin-exchange interactions with lattice-confined polar molecules, *Nature* **501**, 521 (2013).
- [59] B. Zhu, B. Gadway, M. Foss-Feig, J. Schachenmayer, M. L. Wall, K. R. A. Hazzard, B. Yan, S. A. Moses, J. P. Covey, D. S. Jin, J. Ye, M. Holland, and A. M. Rey, Suppressing the loss of ultracold molecules via the continuous quantum Zeno effect, *Phys. Rev. Lett.* **112**, 070404 (2014).
- [60] K. Sponselee, L. Freystatzky, B. Abeln, M. Diem, B. Hundt, A. Kochanke, T. Ponath, B. Santra, L. Mathey, K. Sengstock, and C. Becker, Dynamics of ultracold quantum gases in the dissipative Fermi-Hubbard model, *Quantum Sci. Technol.* **4**, 014002 (2018).
- [61] L. Corman, P. Fabritius, S. Häusler, J. Mohan, L. H. Dogra, D. Husmann, M. Lebrat, and T. Esslinger, Quantized conductance through a dissipative atomic point contact, *Phys. Rev. A* **100**, 053605 (2019).
- [62] O. Gunnarsson and K. Schönhammer, Electron spectroscopies for Ce compounds in the impurity model, *Phys. Rev. B* **28**, 4315 (1983).
- [63] A. J. Daley, Quantum trajectories and open many-body quantum systems, *Advances in Physics* **63**, 77 (2014).
- [64] T. Shi, E. Demler, and J. Ignacio Cirac, Variational study of fermionic and bosonic systems with non-Gaussian states: Theory and applications, *Annals of Physics* **390**, 245 (2018).
- [65] S. Zhang, J. Carlson, and J. E. Gubernatis, Constrained path Monte Carlo method for fermion ground states, *Phys. Rev. B* **55**, 7464 (1997).
- [66] I. Snyman and S. Florens, Efficient impurity-bath trial states from superposed Slater determinants, *Phys. Rev. B* **104**, 195136 (2021).
- [67] A. O. Gogolin, A. A. Nersisyan, and A. M. Tsvelik, *Bosonization and Strongly Correlated Systems* (Cambridge University Press, Cambridge, 1998).
- [68] T. Giamarchi, *Quantum Physics in One Dimension*, 1st ed. (Clarendon Press, Oxford, 2003).
- [69] J. Johansson, P. Nation, and F. Nori, QuTiP: An open-source Python framework for the dynamics of open quantum systems, *Computer Physics Communications* **183**, 1760 (2012).
- [70] J. Johansson, P. Nation, and F. Nori, QuTiP 2: A Python framework for the dynamics of open quantum systems, *Computer Physics Communications* **184**, 1234 (2013).
- [71] M. Foss-Feig, A. J. Daley, J. K. Thompson, and A. M. Rey, Steady-state many-body entanglement of hot reactive fermions, *Phys. Rev. Lett.* **109**, 230501 (2012).
- [72] P. Coleman, *Introduction to Many-Body Physics* (Cambridge University Press, 2015).
- [73] E. H. Lieb and D. W. Robinson, The finite group velocity of quantum spin systems, *Communications in mathematical physics* **28**, 251 (1972).
- [74] M. Nuss, M. Ganahl, E. Arrigoni, W. von der Linden, and H. G. Evertz, Nonequilibrium spatiotemporal formation of the Kondo screening cloud on a lattice, *Phys. Rev. B* **91**, 085127 (2015).
- [75] Y. Ashida, T. Shi, M. C. Bañuls, J. I. Cirac, and E. Demler, Solving quantum impurity problems in and out of equilibrium with the variational approach, *Phys. Rev. Lett.* **121**, 026805 (2018).
- [76] Y. Ashida, T. Shi, M. C. Bañuls, J. I. Cirac, and E. Demler, Variational principle for quantum impurity systems in and out of equilibrium: Application to Kondo problems, *Phys. Rev. B* **98**, 024103 (2018).
- [77] P. Fabritius, J. Mohan, M. Talebi, S. Wili, W. Zwirger, M.-Z. Huang, and T. Esslinger, Irreversible entropy transport enhanced by fermionic superfluidity, *Nature Physics*, 1 (2024).
- [78] J. Mohan, P. Fabritius, M. Talebi, S. Wili, M.-Z. Huang, and T. Esslinger, *Universal entropy transport far from equilibrium across the BCS-BEC crossover* (2024), arXiv:2403.17838 [cond-mat.quant-gas].
- [79] Y. Meir and N. S. Wingreen, Landauer formula for the current through an interacting electron region, *Phys. Rev. Lett.* **68**, 2512 (1992).
- [80] N. S. Wingreen and Y. Meir, Anderson model out of equilibrium: Noncrossing-approximation approach to transport through a quantum dot, *Phys. Rev. B* **49**, 11040 (1994).
- [81] For a particle-hole symmetric AIM, where $\varepsilon_d = -U_d$ in Halmiltonian (3), the SGS approach yields stable, quan-

- tized conductance of $2/h$ after several tunneling time intervals (Γ^{-1}). However, in the case of an asymmetric AIM, the conductance provided by the SGS approach continues to increase slightly beyond $2/h$, even for larger system sizes and extended simulation time.
- [82] H. Haug, A.-P. Jauho, *et al.*, *Quantum kinetics in transport and optics of semiconductors*, Vol. 2 (Springer, 2008).
- [83] H.-P. Breuer and F. Petruccione, *The Theory of Open Quantum Systems* (Oxford University Press, Oxford, 2003).
- [84] We notice that if $\gamma \gg V$ but V is sufficiently larger than the bandwidth of the leads, the transitions to the bright states are highly off-resonant and thus suppressed—but in a more usual, Hamiltonian way.
- [85] J. J. García-Ripoll, S. Dürr, N. Syassen, D. M. Bauer, M. Lettner, G. Rempe, and J. I. Cirac, Dissipation-induced hard-core boson gas in an optical lattice, *New Journal of Physics* **11**, 013053 (2009).
- [86] E. M. Kessler, Generalized Schrieffer-Wolff formalism for dissipative systems, *Phys. Rev. A* **86**, 012126 (2012).
- [87] N. E. Bickers, Review of techniques in the large- N expansion for dilute magnetic alloys, *Rev. Mod. Phys.* **59**, 845 (1987).
- [88] P. Nozières and A. Blandin, Kondo effect in real metals, *J. Phys. France* **41**, 193 (1980).
- [89] B. A. Jones, C. M. Varma, and J. W. Wilkins, Low-temperature properties of the two-impurity Kondo Hamiltonian, *Phys. Rev. Lett.* **61**, 125 (1988).
- [90] I. Affleck and A. W. W. Ludwig, Exact critical theory of the two-impurity Kondo model, *Phys. Rev. Lett.* **68**, 1046 (1992).
- [91] I. Affleck and A. W. W. Ludwig, Exact conformal-field-theory results on the multichannel Kondo effect: Single-fermion Green’s function, self-energy, and resistivity, *Phys. Rev. B* **48**, 7297 (1993).
- [92] A. Bayat, H. Johannesson, S. Bose, and P. Sodano, An order parameter for impurity systems at quantum criticality, *Nature communications* **5**, 3784 (2014).
- [93] A. Keller, L. Peeters, C. Moca, I. Weymann, D. Mahalu, V. Umansky, G. Zaránd, and D. Goldhaber-Gordon, Universal Fermi liquid crossover and quantum criticality in a mesoscopic system, *Nature* **526**, 237 (2015).
- [94] Z. Iftikhar, S. Jezouin, A. Anthore, U. Gennser, F. Parmentier, A. Cavanna, and F. Pierre, Two-channel Kondo effect and renormalization flow with macroscopic quantum charge states, *Nature* **526**, 233 (2015).
- [95] Z. Iftikhar, A. Anthore, A. Mitchell, F. Parmentier, U. Gennser, A. Ouerghi, A. Cavanna, C. Mora, P. Simon, and F. Pierre, Tunable quantum criticality and super-ballistic transport in a “charge” Kondo circuit, *Science* **360**, 1315 (2018).
- [96] S. Lorenzo, J. Marino, F. Plastina, G. M. Palma, and T. J. Apollaro, Quantum critical scaling under periodic driving, *Scientific reports* **7**, 5672 (2017).
- [97] W. Pouse, L. Peeters, C. L. Hsueh, U. Gennser, A. Cavanna, M. A. Kastner, A. K. Mitchell, and D. Goldhaber-Gordon, Quantum simulation of an exotic quantum critical point in a two-site charge Kondo circuit, *Nature Physics* **19**, 492 (2023).
- [98] V. J. Emery and S. Kivelson, Mapping of the two-channel Kondo problem to a resonant-level model, *Phys. Rev. B* **46**, 10812 (1992).
- [99] J. Gan, Mapping the critical point of the two-impurity Kondo model to a two-channel problem, *Phys. Rev. Lett.* **74**, 2583 (1995).
- [100] E. Sela, A. K. Mitchell, and L. Fritz, Exact crossover Green function in the two-channel and two-impurity Kondo models, *Phys. Rev. Lett.* **106**, 147202 (2011).
- [101] A. K. Mitchell, E. Sela, and D. E. Logan, Two-channel Kondo physics in two-impurity Kondo models, *Phys. Rev. Lett.* **108**, 086405 (2012).
- [102] A. K. Mitchell and E. Sela, Universal low-temperature crossover in two-channel Kondo models, *Phys. Rev. B* **85**, 235127 (2012).
- [103] L. A. Landau, E. Cornfeld, and E. Sela, Charge fractionalization in the two-channel Kondo effect, *Phys. Rev. Lett.* **120**, 186801 (2018).
- [104] D. B. Karki, E. Boulat, W. Pouse, D. Goldhaber-Gordon, A. K. Mitchell, and C. Mora, F_3 parafermion in the double charge Kondo model, *Phys. Rev. Lett.* **130**, 146201 (2023).
- [105] W. Hofstetter and H. Schoeller, Quantum phase transition in a multilevel dot, *Phys. Rev. Lett.* **88**, 016803 (2001).
- [106] M. Pustilnik and L. I. Glazman, Kondo effect in real quantum dots, *Phys. Rev. Lett.* **87**, 216601 (2001).
- [107] W. G. van der Wiel, S. De Franceschi, J. M. Elzerman, S. Tarucha, L. P. Kouwenhoven, J. Motohisa, F. Nakajima, and T. Fukui, Two-stage Kondo effect in a quantum dot at a high magnetic field, *Phys. Rev. Lett.* **88**, 126803 (2002).
- [108] G. Granger, M. A. Kastner, I. Radu, M. P. Hanson, and A. C. Gossard, Two-stage Kondo effect in a four-electron artificial atom, *Phys. Rev. B* **72**, 165309 (2005).
- [109] D. B. Karki, C. Mora, J. von Delft, and M. N. Kiselev, Two-color Fermi-liquid theory for transport through a multilevel Kondo impurity, *Phys. Rev. B* **97**, 195403 (2018).
- [110] X. Guo, Q. Zhu, L. Zhou, W. Yu, W. Lu, and W. Liang, Evolution and universality of two-stage Kondo effect in single manganese phthalocyanine molecule transistors, *Nature communications* **12**, 1566 (2021).